**Title page**

# Quartz-Seq2: a high-throughput single-cell RNA-sequencing method that effectively uses limited sequence reads

Yohei Sasagawa[1†], Hiroki Danno[1†], Hitomi Takada[2†], Masashi Ebisawa[1], Tetsutaro Hayashi[1], Akira Kurisaki[2*], and Itoshi Nikaido[1,3*]

[†]Contributed equally

*Corresponding author

[1]Bioinformatics Research Unit, Advanced Center for Computing and Communication, RIKEN, Hirosawa 2-1, Wako, Saitama, Japan

[2]Laboratory of Stem Cell Technology, Graduate School of Biological Sciences, Nara Institute of Science and Technology, Takayama-cho 8916-5, Ikoma, Nara, Japan

[3]Single-cell Omics Research Unit, RIKEN Center for Developmental Biology. 2-2-3 Minatojima-minamimachi, Chuou-ku, Kobe, Japan

Yohei Sasagawa: youhei.sasagawa@riken.jp

Hiroki Danno: hiroki.danno@riken.jp, redgrapefruit@mac.com

Hitomi Takada: htakada@bs.naist.jp

Masashi Ebisawa: masashi.ebisawa@riken.jp

Tetsutaro Hayashi: tetsutaro.hayashi@riken.jp

Akira Kurisaki: akikuri@bs.naist.jp

Itoshi Nikaido: itoshi.nikaido@riken.jp

**Abstract**

High-throughput single-cell RNA-seq methods assign limited unique molecular identifier (UMI) counts as gene expression values to single cells from shallow sequence reads and detect limited gene counts. We thus developed a high-throughput single-cell RNA-seq method, Quartz-Seq2, to overcome these issues. Our improvements in several of the reaction steps of Quartz-Seq2 allow us to effectively convert initial reads to UMI counts (at a rate of 30%–50%). To demonstrate the power of Quartz-Seq2, we analyzed transcriptomes from a cell population of *in vitro* embryonic stem cells and an *in vivo* stromal vascular fraction with a limited number of sequence reads.

**Keywords**

High-throughput single-cell RNA-seq

Flow-cytometry

Cell sorter

Quartz-Seq

Poly-A tagging

Stromal vascular fraction

Mesenchymal stem cell

## Background

Single-cell transcriptome analysis allows us to identify nongenetic cellular heterogeneity, which includes differences in cell type due to differentiation and differences in cell state within a cell population. In previous studies, various methods for single-cell RNA-seq were developed [1-19]. Some of these that generate read coverage across all transcripts have been exploited to detect alternative transcription splicing isoforms [14,17] and others using unique molecular identifier (UMI) have been applied to quantify the number of transcripts expressed in a cell [1-3,6,7,9,11-13,20]. To extract substantial information on a cell population, such as the composition of different cell types or the distribution of cell states, it is necessary to analyze hundreds or thousands of cells. Cell barcoding is a key technology for this, which enables us to deal with samples from numerous cells in a single tube. Cell barcoding technology, which tags nucleotides unique to each cell to target RNA molecules from that cell, is a key technology for increasing the throughput of single-cell RNA-seq [16,18]. Mixing cDNA tagged with cell barcodes before whole-transcript amplification decreases the cost of reaction reagents and the laboriousness of experimental steps. There are two types of cell barcoding technology according to the method of cell sampling used. One method involves single cells being selectively sorted to multi-well plates using flow cytometry, which allows us to remove dead or aggregated cells. Besides, transcriptome data can be linked to cellular information measured in flow cytometry. The other method involves single cells and barcoded beads being captured in water-in-oil droplets using droplet-generation microfluidic devices [6,7]. In this latter method, thousands of cells can probabilistically be captured in half an hour. However, the total number of sequence reads generated by a deep sequencer is still limited. To increase the number of analyzed cells, each cell is assigned a limited number of initial sequence reads. For example, approximately 400 million initial reads were sequenced for 3,000–4,000 cells in several previous studies [6,7]. UMI counts were converted from initial sequence reads for each cell, and the conversion ratio of that was limited to approximately one-tenth [21]. Ideally, greater UMI counts should be generated from limited sequence reads because the increase in UMI count assigned to each cell leads to the detection of low-copy genes and the identification of cell-type-specific genes using statistical tests.

In this study, we developed a novel high-throughput single-cell RNA-seq method, Quartz-Seq2. As Quartz-Seq is a sensitive and reproducible single-cell RNA-seq method, Quartz-Seq2 was developed based on it [15]. Quartz-Seq is based on a poly-A tagging strategy. By the combination of molecular biological improvements including major improvement of poly-A tagging, Quartz-Seq2 resulted in an increase in the effectiveness with which the initial sequence reads were converted to the expression UMI counts (UMI conversion efficiency: 30%–50%). To demonstrate the highly effective use of initial reads in Quartz-Seq2, we analyzed a population of mouse embryonic stem (ES) cells as *in vitro* cells and the cell population from the stromal vascular fraction (SVF) as *in vivo* cells.

146 **Results**

147

148 **Outline of Quartz-Seq2 experiment**

149 To increase the UMI conversion efficiency, we improved several steps in the preparation of the
150 single-cell RNA-seq library (Additional file 1: Figure S1), resulting in the development of
151 Quartz-Seq2. Below, we explain the five steps of the Quartz-Seq2 procedure (Figure 1).

152 (1) The first step is single-cell collection using a cell sorter. We selectively sort living
153 single cells into lysis buffer in a 384-well PCR plate without dead cells. In cell sorting, various
154 types of channel information, such as the intensity of fluorescence, are measured for each cell.
155 This enables us to link the transcriptome to cellular information from a cell sorter for each cell.

156 (2) The second step is cell barcoding. Each well contains lysis buffer and
157 reverse-transcription (RT) primer, which includes a cell barcode sequence (14- or 15-mer), a
158 UMI sequence (8-mer), and an oligo-dT sequence (24-mer). Using these RT primers,
159 respective RNA from single cells is converted to cDNA with unique cell barcodes. Note that a
160 long RT primer resulted in a severe problem regarding the synthesis of byproducts at the
161 downstream reaction in our system (Additional file 1: Figure S2 and Supplemental Note).
162 Therefore, we use a relatively short RT primer (73- or 74-mer), which allows us to skip the step
163 of removing byproducts using exonuclease I. We design two types of RT primer set (v3.1: 384
164 barcodes; v3.2: 1536 barcodes). Within each primer set, barcode sequences are designed
165 such that the minimum Sequence–Levenshtein distance between two sequences should be
166 greater than 5, which leads to the correction of two nucleotides of mismatch, insertion and
167 deletion in sequence reads [22]. We also optimize the buffer and temperature in the RT
168 reaction, leading to an improvement of RT efficiency from that of the original Quartz-Seq
169 (Additional file 1: Figure S3 and Supplemental Note).

170 (3) The third step involves the pooling of cell-barcoded cDNA. By cell barcoding,
171 Quartz-Seq2 can pool cDNA of up to 1,536 individual cells into one mixture. We developed a
172 rapid and high-throughput method for collecting small volumes of cDNA in multiwell plates. This
173 method also achieved higher efficiency of collection than dispensing with pipettes and tips
174 (Additional file 1: Figure S4 and Supplemental Note). As the efficiency of cDNA purification

175 after pooling was 93.77%, we estimated that approximately 80% of cell-barcoded cDNA could
176 be used for subsequent whole-transcript amplification in our system (Additional file 1: Figure
177 S3a and Supplemental Note).
178 (4) The fourth step is whole-transcript amplification based on an improved poly-A tagging
179 strategy. Poly-A tagging is one of the methods of converting first-strand cDNA to amplifiable
180 cDNA. First-strand cDNA is extended with a poly-A tail by the terminal transferase.
181 Subsequently, second-strand cDNA is synthesized with tagging primers that contain a poly-dT
182 sequence, followed by PCR amplification. Here, we improve the efficiency of poly-A tagging by
183 3.6-fold. This improvement is a crucial point in the development of Quartz-Seq2. We describe
184 the details of this in the next subsection.
185 (5) The fifth step is library preparation for deep sequencing. Amplified cDNA is
186 fragmented, ligated with the sequence adapter, and amplified by PCR. In sequencing using
187 Illumina sequencers, a sequence for a cell barcode and a UMI is read in Read1, while a
188 sequence for a region of a transcript (mRNA) is read in Read2.
189
190 **Improvement of poly-A tagging efficiency**
191 We previously reported Quartz-Seq based on the poly-A tagging strategy, which has a
192 significant potential for detecting a large number of genes expressed in a cell [15]. However,
193 the efficiency of poly-A tagging itself for single-cell RNA-seq has not been improved. We
194 hypothesized that the improvement of poly-A tagging would lead to high UMI conversion
195 efficiency. Therefore, we attempted to improve the efficiency of this tagging step. Poly-A
196 tagging is composed of two processes: (1) The first-strand cDNA is modified with a poly-A tail
197 by terminal deoxynucleotidyl transferase. (2) Next, the poly-A-tailed cDNA is annealed with a
198 tagging primer, which has a poly-dT sequence. Then, the second-strand cDNA is extended.
199 The resulted second-strand cDNA is amplifiable cDNA, which has a PCR primer sequence at
200 both ends of it.
201 It is known that the DNA yield of amplified cDNA generally reflects the quantitative
202 performance of single-cell RNA-seq methods [3,13,14]. Thus, we determined the effects of
203 various buffers for the poly-A tailing step on the amplified cDNA yield. We performed the poly-A

204 tailing reaction with various buffers using purified first-strand cDNA from 1 ng of total RNA
205 (Figure 2a, Additional file 1: Figure S5). Finally, we obtained amplified cDNA. We found that the
206 use of T55 buffer and RH55 buffer in the poly-A tailing reaction efficiently improved the cDNA
207 yield (Figure 2a). The amount of amplified cDNA increased 2.88-fold and 2.55-fold using T55
208 buffer and RH55 buffer, respectively, compared with the level using Quartz-Seq buffer (Figure
209 2a). In these buffer conditions, we did not observe any obvious byproducts derived from the RT
210 primer (Figure 2a, Additional file 1: Figures S2 and S5, and Supplemental Note).
211 Next, we added an “Increment” temperature condition for the tagging and second-strand
212 synthesis steps (see Material and Methods). In this condition, the reaction temperature of these
213 steps was gradually increased. As a result, the amount of cDNA tended to increase, by
214 approximately 1.2-fold (Figure 2a). Moreover, upon combining T55 buffer and the Increment
215 condition, the amount of cDNA increased approximately 3.6-fold. We also confirmed the
216 reproducibility of this phenomenon of cDNA increment in the additional experiments (Additional
217 file 1: Figure S5). Moreover, we confirmed the amplified cDNA yield of various genes by qPCR
218 analysis as another assay. Specifically, we determined the qPCR scores of eight genes from
219 amplified cDNA and nonamplified cDNA (Figure 2b). Spearman's rank correlation coefficients
220 (SCCs) between amplification and nonamplification were approximately 0.79 in both conditions
221 (T55+Increment, RH55+Increment). The SCC was approximately 0.66 in Quartz-Seq-like
222 conditions. We also observed clear increments of qPCR scores for almost all genes. These
223 results show that the combination of T55 buffer and this temperature condition improved the
224 efficiency of the poly-A tagging step. We also found that other conditions (NBF40+Increment)
225 improved the cDNA yield. However, under these conditions, byproducts were clearly
226 synthesized (Additional file 1: Figures S4c and S5b). Moreover, the cDNA amount with T55
227 buffer was slightly greater than the cDNA amount with RH55 (Figure 2 and Additional file 1:
228 Figure S5a). Therefore, we used the combination of T55 buffer and the “Increment”
229 temperature condition for the poly-A tagging strategy.
230
231 **Evaluation of the quantitative performance of Quartz-Seq2 using single-cell total RNA**

232 Finally, we adopted three molecular-biological improvements [modified RT condition, poly-A
233 tailing buffers (T55), and the “Increment” temperature condition] for Quartz-Seq2 (Additional file
234 1: Figure S1). To determine the technical variability and specificity of Quartz-Seq2, we
235 performed whole-transcript amplification using 10 pg of diluted mouse total RNA as a
236 single-cell-like averaged sample with the v3.1 384 cell-barcode RT primer in a 384-well plate.
237 In this experiment, we used the “RT100” enzyme concentration for reverse transcription. The
238 effect of enzyme concentration is specifically described in the next subsection of this paper. We
239 analyzed 10 pg of total RNA in all wells at approximately 0.19 M fastq reads on average per
240 well. In the case of Quartz-Seq-like conditions, we detected 19,614±3516 UMI counts and
241 5726±494 gene counts (n=384 wells). In the case of Quartz-Seq2, we achieved a UMI count of
242 35,391±8719 and a gene count of 6,621±711 (n=384 wells). We confirmed the reproducibility
243 of the quantitative performance by a further batch experiment with other 384-well plates, which
244 had 10 pg of total RNA in all wells (Additional file 1: Figure S6). These results indicated that the
245 combination of the three molecular-biological improvements for Quartz-Seq2 clearly improved
246 the conversion ratio from target RNA to sequence library DNA. We also confirmed the
247 correlation between single-cell RNA-seq data and bulk RNA-seq data. SCC between
248 Quartz-Seq2 and bulk RNA-seq was 0.85 (Figure 2d). This result indicates that Quartz-Seq2
249 data are comparable to conventional bulk RNA-seq data. We also determined the variability of
250 expression between technical replicates to investigate the UMI filtering effect. The mean-CV
251 (coefficient of variation) plot of Quartz-Seq2 clearly showed that UMI filtering reduced
252 expression variability derived from PCR bias (Figure 2e). Moreover, technical gene expression
253 variability of Quartz-Seq2 became fairly close to the theoretical variability of a Poisson
254 distribution (Figure 2e).
255 We also focused on the relationship between sequencing platform and Quartz-Seq2.
256 We did not observe clear differences between the NextSeq500 and HiSeq2500 sequencing
257 platforms for determination of the UMI count and the gene count for Quartz-Seq2 (Additional
258 file 1: Figure S7a). On the other hand, the unique mapping ratio and UMI count clearly
259 depended on the Read2 length for transcript mapping (Additional file 1: Figure S7c, d). In this
260 regard, the number of detected genes slightly depended on Read2 length (Additional file 1:

261 Figure S7d). Long Read2 length led to better UMI counts, but high sequencing cost (Additional
262 file 1: Figure S7b). Therefore, in this study, we mainly used the NextSeq500 sequence platform
263 and a Read2 length of 62 due to the cost performance of this combination. Moreover, we
264 mainly used the adaptor ligation method for sequence library preparation of Quartz-Seq2. We
265 did not observe a clear difference between the two sequence library preparation methods
266 (ligation and Nextera/Tn5 transposase) regarding determination of the UMI count and the gene
267 count. However, we could easily identify specific familiar genes (such as *Pou5f1* and *Gapdh*)
268 using the ligation method (Additional file 1: Figure S7e). Therefore, we mainly used the ligation
269 method for Quartz-Seq2.
270
271 **Reduction of enzyme concentration in reverse transcription decreased cost and**
272 **technical noise of Quartz-Seq2**
273 The cost of experimental preparation per cell was approximately ¥2,600 ($23) for our
274 previously reported Quartz-Seq, which does not use cell barcoding (Figure S8c). As mentioned
275 earlier, we used the “RT100” enzyme condition in reverse transcription for Quartz-Seq2. This
276 enzyme concentration in RT reaction is broadly used for various molecular biological
277 application including single-cell RNA-seq methods. By using the cell barcoding strategy, the
278 cost of experimental preparation for Quartz-Seq2 under the “RT100” condition was reduced
279 (¥121 or $1.08 per cell)(Additional file 1 Figure S8c). We found that 65% of the cost in
280 experimental steps is derived from reverse transcription in Quartz-Seq2 under the “RT100”
281 condition (Figure 3a). To further reduce the cost of experimental preparation of sequence
282 libraries on large scale, we investigated the effect of a low enzyme concentration in reverse
283 transcription in Quartz-Seq2. In the assessment assay, we noticed that a low enzyme
284 concentration did not markedly affect the efficiency of reverse transcription and the amount of
285 amplified cDNA yield (Figure S8a right panel and S8b). Therefore, we prepared three technical
286 replicates of a 384-well PCR plate with 10 pg of total RNA with the “RT100” condition or the
287 “RT25” low-enzyme condition. In the “RT25” condition, the amount of cDNA yield showed a
288 tendency for a slight increase of approximately 1.17-fold, which although not being a major

289 improvement did at least not involve a decrease. The cost of experimental preparation per cell
290 became approximately ¥45–¥62 ($0.4–$0.55) in the “RT25” condition.
291 We validated the quantitative performance with 10 pg of total RNA in the “RT100” and
292 “RT25” conditions at various input data sizes. Unexpectedly, we found that the “RT25”
293 condition improved the quantitative performance (Figure 3c and Additional file 1: Figure S9). In
294 a typical pattern, approximately 4,000 single cells were analyzed by the NextSeq500
295 sequencer in the high-throughput single-cell RNA-seq method [6,7,21]. In this case, the input
296 data size for a single cell involves shallow initial reads (0.1 M fastq reads) (Figure 3d). We
297 compared RT25 with RT100 at approximately 0.096 M fastq reads on average per well. In the
298 case of Quartz-Seq2 in the “RT25” condition, we achieved a UMI count of 30,117±789 and a
299 gene count of 6,320±35 (n=3 plates). In the case of Quartz-Seq2 in the “RT100” condition, we
300 achieved a UMI count of 25,671±1020 and a gene count of 5,889±35 (n=3 plates). The capture
301 ratios of ERCC spike were 11.49±0.46% and 10.28±0.31% in the “RT25” and “RT100”
302 conditions, respectively (Figure 3d and e). In addition, the capture ratio of ERCC spike was
303 16.38±0.66% in the “RT25” condition at approximately 0.27 M fastq reads on average per well
304 (Figure 3c, e). We also investigated the technical variability of UMI count and gene count. The
305 well-to-well technical variability for UMI count and gene count clearly decreased in the “RT25”
306 condition (Figure 3). These results showed that the “RT25” low-enzyme condition clearly
307 reduced the experimental cost and improved the quantitative performance, including that for
308 the UMI count. We thus applied the “RT25” condition in subsequent experiments using real
309 single cells.
310
311 **Quartz-Seq2 shows high efficiency of UMI conversion**
312 The increase of UMI counts generated from limited initial sequence reads leads to the
313 detection of low-copy genes and the identification of more marker genes using statistical tests.
314 We calculated the UMI conversion efficiency, which indicates how effectively initial reads can
315 be converted to UMI counts (Figure 4a and Additional file 1: Figure S10). The UMI conversion
316 efficiency of Quartz-Seq2 with 10 pg of purified total RNA (from mouse ES cells) ranged from
317 31% to 39% at approximately 0.096 M initial reads depending on the Read2 length.

318 We performed Quart-Seq2 and Drop-seq on a mixture of mouse ES cells and the
319 Dex-treated mouse ES cells (primitive endoderm (PrE) cells), and calculated the UMI
320 conversion efficiency (Figure 4b and Additional file 1: Figure S11a). Drop-seq is one of the
321 high-throughput single-cell RNA-seq methods, which can capture thousands of cells and
322 barcoded beads in half an hour [6]. We performed Drop-seq experiments, which were validated
323 by species-mixing analysis (Figure S11b, c). The effectiveness of Quartz-Seq2 ranged from
324 25% to 35% depending on the initial read depth (Figure 4), which was higher than that of
325 Drop-seq.
326 As Figure 4b shows, Quartz-Seq2 detected more genes with high UMI conversion
327 efficiency. To examine the power for identifying marker genes, we performed principal
328 component analysis (PCA) and clustering. The number of genes differentially expressed
329 between two distinct cell types was calculated (ES and PrE cells) (Additional file 1: Figure
330 S11d). The results showed that more genes that were differentially expressed between the two
331 cell types were identified with Quartz-Seq2 (Figure 4b). In addition, more biological pathways
332 particularly associated with the differentially expressed genes were detected in Quartz-Seq2
333 (Figure 4c). Furthermore, we calculated genes with highly variable expression in Quartz-Seq2
334 and Drop-seq, which potentially include not only genes that are differentially expressed
335 between cell types but also genes of which the expression changes depending on the cell state
336 in a cell type. The results also showed that more Gene Ontology (GO) terms enriched among
337 the genes with highly variable expression were identified with Quartz-Seq2. Terms on cell cycle
338 state were only enriched in the genes calculated with Quartz-Seq2 (Figure 4d). These results
339 suggest that high UMI conversion efficiency with limited initial reads leads to more biological
340 information being revealed, such as functional terms and biological pathways.
341 To obtain additional evidence for the superiority of Quartz-Seq2 in terms of the UMI
342 conversion efficiency and gene count, we compared Quartz-Seq2 to other methods. Using
343 mouse ES cells, Ziegenhain et al. systematically compared the quantitative performance of
344 several single-cell RNA sequencing (RNA-seq) methods [CEL-seq2(C1), SCRB-seq,
345 MARS-seq, and Drop-seq] that use the UMI technique [21]. For comparison between our and
346 their data, we reanalyzed our Quartz-Seq2 data from mouse ES cells using their analysis

347 condition. The results indicate that the UMI conversion efficiency of the Quartz-Seq2 method
348 was approximately 34.3 ± 0.7% (n = 4); the UMI conversion efficiency of the other methods
349 ranged from 7 to 23%. The gene count using Quartz-Seq2 was approximately 6,722 ± 57 (n =
350 4), while the average gene counts for the other methods ranged from 2,700 to 5,200. In
351 particular, the UMI conversion efficiency and gene count of the Quartz-Seq2 method were
352 significantly better than those of the other methods at approximately 0.1 million initial reads
353 (Figure 5a and Additional file 1: Figure S12). We also estimated the UMI and gene counts and
354 the UMI conversion efficiency at various numbers of initial fastq reads (Figure 5b). We found
355 that Quartz-Seq2 is greatly advantageous for detecting the UMI and gene counts from limited
356 initial amounts of data (under 0.25 million fastq reads).
357
358 **Quartz-Seq2 achieves high UMI conversion efficiencies at relatively low costs**
359 As mentioned earlier, the experimental cost of Quartz-Seq2 for library preparation ranges from
360 ¥45–62 ($0.4–0.55). In terms of the cost, Quartz-Seq2 is highly competitive with other
361 single-cell RNA-seq methods that use a cell sorter (Additional file 1: Figure S8c). We estimate
362 that the number of processable single cells per 1,000 dollars spent on Quartz-Seq2 ranges
363 from 1,800 to 2,500 (Figure 5a). We also calculated the total cost, including the sequencing
364 and library preparation costs, for each method. The total cost per cell is extremely low
365 (approximately ¥71–131, or $0.63–1.16) for Drop-seq. The total cost per cell is ¥105–165
366 ($0.94–1.47) for Quartz-Seq2. We note that the total cost of Quartz-Seq2, a cell sorter–based
367 method, approaches that typical of droplet-based methods (Additional file 1: Figure S8d). The
368 Quartz-Seq2 method achieves highest UMI conversion efficiency at limited numbers of initial
369 reads, providing single-cell RNA-seq data in a high-throughput manner.
370
371 **Quartz-Seq2 analysis on 4,484 mouse embryonic stem cells in maintenance and**
372 **differentiated conditions**
373 We did not observe any clear differences in UMI counts and gene counts between the v3.1 and
374 v3.2 RT primer sets (Additional file 2: Table S1). To demonstrate the capability of Quartz-Seq2
375 for quantifying the transcriptome of a large number of cells and identifying rare cell populations,

376 we analyzed approximately 4,484 cells from a mixture of mouse ES cells and
377 differentiation-induced cells. Cells were prestained with Hoechst 33342 and/or Calcein-AM as
378 an indicator of DNA content and culture condition (ES or PrE cells), respectively (Figure 6a).
379 Calcein-AM-positive and -negative cells were sorted to 12 of 384-well plates in a checkered
380 pattern (Figure 6a). In this condition, the cell doublets caused by mis-sorting can be detected at
381 the highest probability. In this analysis, as an average for cells, 0.1 M initial fastq reads were
382 effectively converted to 35,915±1,188 UMI counts in a final gene expression matrix. The UMI
383 conversion efficiency was 35.91±1.18%.
384 Dimensionality reduction of the expression UMI matrix resulting from Quartz-Seq2
385 showed clear separation of six clusters, including the main populations of ES cells and PrE
386 cells and four small populations. We did not observe a clear batch effect between 12 of the
387 384-well plates (Additional file 1: Figure S13). One cluster contained a relatively high ratio of
388 mitochondrial RNA (Additional file 1: Figure S14), which was judged to reflect low-quality cells
389 [23]. Another cluster showed high values of detected UMI counts and gene counts, and
390 expressed both ES and PrE marker genes, which were judged to represent doublets of an ES
391 cell and a PrE cell. To characterize the identified populations, we determined the genes that
392 were specific or enriched for each cluster using binomial tests (Figure 6c and Additional file 1:
393 Figure S15). Although cells in cluster 3 shared gene expression with the main population of ES
394 cells (cluster 1), some genes including *Stmn2* and *Rhox5* were additionally expressed,
395 suggesting that cluster 1 and cluster 3 shared the same cell type but had different cell states.
396 Cluster 5 was a small population (0.17%, Figure 6b), but was characterized by many specific
397 marker genes (Figure 6b), including *Zscan4c* and *Zscan4d*, which are known to be expressed
398 in a subpopulation of mouse ES cells [24]. However, among our culture conditions, these
399 genes were more expressed in the Dex-treatment condition than in the ES-maintenance
400 condition. Flow cytometry information on cells in cluster 5 also showed no fluorescence of
401 Calcein-AM, indicating that these cells were from the suspension of Dex-treated cells (Figure
402 6d). These observations were consistent with a previous study demonstrating that *Zscan4* was
403 more expressed in a differentiation condition induced by withdrawal of leukemia inhibitory
404 factor [7].

405 In sampling of cells using a cell sorter, flow cytometry information including the intensity
406 of Hoechst 33342 staining for each cell was collected. Using this information, we reconstructed
407 the distribution of Hoechst 33342 staining intensity for each cluster (Figure 6e). The main
408 population of ES cells (cluster 1) showed an embryonic pattern of distribution of DNA content,
409 which is characterized by a high ratio of cells in G2 and M phases to cells in the G1 phase. On
410 the other hand, the main population of PrE cells (cluster 4) showed a somatic pattern of
411 distribution of DNA content. This was consistent with PrE cells being differentiated from ES
412 cells. The cells in cluster 3, the gene expression of which was similar to that of the ES main
413 population (cluster 1), showed an embryonic pattern rather than a somatic one. As the number
414 of cells in cluster 5 that expressed *Zscan4c/d* was small, it was difficult to classify the observed
415 pattern as the embryonic or somatic type. These findings indicated the usefulness of single-cell
416 RNA-seq using flow cytometry for the reconstruction of population information after
417 transcriptome-based clustering. For good interpretation of the distribution, a large number of
418 cells for each cluster are required.
419
420 **Quartz-Seq2 revealed two types of cell state: cell cycle-dependent and -independent**
421 **heterogeneity**
422 When cells were plotted on t-SNE (t-distributed stochastic neighbor embedding) space using
423 transcriptome analysis and the intensity of Hoechst 33342 staining was colored, the gradient
424 pattern was easily observed for clusters 1, 3, and 4 (Figure 7a), suggesting that Quartz-Seq2
425 was highly sensitive for detection of the cell cycle state. To examine this, we plotted the gene
426 expression of several cell cycle markers against the intensity of Hoechst 33342 staining, which
427 indicated the strong dependence of such expression on DNA content (Figure 7b). Using the
428 intensity of Hoechst 33342 staining, cell cycle dependence was calculated for all genes
429 detected in Quartz-Seq2 experiments, resulting in the identification of numerous genes for
430 which the expression level changed depending on the DNA content (Figure 7c, d and
431 Additional file 1: Figure S16). We called these genes cell cycle-associated genes. Again, it was
432 confirmed that the ratio of cells in G1 and S phases to those in G2 and M phases was different
433 between ES and PrE cells (Figure 7c). As we showed that the efficiency of UMI conversion was

434 high in the Quartz-Seq2 method, we examined whether 10,000 initial reads are sufficient for
435 cell cycle analysis (Additional file 1: Figure S17). In this analysis, final UMI count was 4,774±62
436 and the UMI conversion efficiency was 47.74±0.66%. Plotting cells on t-SNE space with
437 coloring the intensity of Hoechst 33342 staining revealed a gradient pattern, which was
438 positively correlated with G2/M marker genes including *Ccnb1* and *Top2a* and was negatively
439 correlated with G1-phase marker genes such as *Ccne1* (Additional file 1: Figure S17). These
440 observations demonstrated Quartz-Seq2 with few initial sequence reads could analyze cell
441 cycle due to the high UMI conversion efficiency.
442 Within a single cell type, there are two types of cell state. One is the different stages of
443 the cell cycle as mentioned above, and the other refers to cellular heterogeneity that is only
444 remotely related to the cell cycle phases. This means that genes with variable expression in a
445 cell type include cell cycle-associated genes and gene with variable expression that is
446 independent of the cell cycle phases (cell cycle-phase independent variable genes). We
447 determined the number of this latter group of genes by subtracting the cell cycle-associated
448 genes from the genes with variable expression (Figure 7e). For the main population of ES cells
449 (cluster 1), we identified tens of cell cycle-phase independent variable genes. These genes
450 included *Spp1*, *Rhox5*, and *S100a6*, which were previously identified as genes with highly
451 variable expression by scRNA-seq (Figure 7) [7,13,15]. We also identified *Stmn2*, *Dnmt3l*,
452 *Tmsb4x*, and several genes as novel cell cycle phase-independent variable genes. Single-cell
453 RT-qPCR also showed high variability for *Stmn2* and *Rhox5* compared with that for *Nanog*
454 (Figure 7f). In previous studies, *Sgk1* and *Actb* were identified as genes with variable
455 expression by scRNA-seq that analyzed cells only in G1 phase or cells without measuring the
456 intensity of Hoechst 33342 [7,15]. In this study, these were classified as cell cycle-associated
457 genes (Additional file 1: Figure S16).
458 These results show that Quartz-Seq2 globally classified genes with variable expression
459 within a cell type into cell cycle-associated genes and cell cycle phase-independent genes with
460 variable expression by using Hoechst 33342 staining intensity data obtained in flow cytometry.
461

462 **The global picture of cell-type composition in stromal vascular fraction as revealed by**
463 **Quartz-Seq2**
464 Next, Quartz-Seq2 was applied to cells from the mouse stromal vascular fraction (SVF), which
465 was taken from adipose tissue (Figure 8a). SVF is thought to be one of the most important
466 sources of mesenchymal stem cells (MSC) due to its potential for cell therapies and the
467 stimulation of endogenous repair [25-28]. However, the global picture of cell-type composition
468 in SVF has not been clarified. To do so, we first observed the distribution of cell size in the SVF
469 population and found it to be broad (5–13 μm, average 6.43 ± 1.35 μm; n=200) (Figure 8a).
470 This was confirmed by flow cytometry data that were obtained using a cell sorter. It is known
471 that the typical amount of total RNA in a mammalian cell is approximately 10 pg [15,17]. Thus,
472 the average amount of total RNA in the SVF population of approximately 1.7 pg is relatively
473 small.
474 We collected cells in multiple 384-well PCR plates and analyzed their transcriptome
475 using Quartz-Seq2. In this analysis, 38,450±3513 initial fastq reads were converted to UMI
476 counts in the final digital expression matrix. The UMI conversion efficiency was 26.85±2.70%
477 (n=3). We observed broader distributions of UMI counts and gene counts in SVF than in ES
478 and 10 pg of total RNA. The gene counts correlated well with side scatter (SSC) values, which
479 were associated with cell size (Additional file 1: Figure S19).
480 Dimensionality reduction and clustering of single-cell transcriptome data showed the
481 clear separation of 11 clusters (Figure 8b). To annotate the cell type on each cluster, we
482 calculated marker genes and functional terms that were either specific or enriched for each
483 cluster (Figure 8c, d and Additional file 1: Figures S18 and S20). As Figure 8c shows, clusters 1,
484 2, 5, and 8-11 expressed cluster-specific genes, and clusters 3, 4, 6, 7, and 9 shared
485 expressed genes (marker class C) as well as differentially expressed genes of classes D-G.
486 Taking these markers and functional terms as well as previous knowledge together, each
487 cluster was identified as follows: two types of *Cd34*-positive MSC (cluster 1: 7.8%, cluster 8:
488 6.4%), two types of *Cd4*-positive T cells (cluster 3: 45.0%, cluster 4: 1.0%), *Cxcr6*-positive T
489 cells (cluster 9: 1.71%), B cells (cluster 5: 15.9%), killer T cells (cluster 6: 11.0%), natural killer
490 cells (cluster 7: 3.0%), macrophages (cluster 2: 5.5%), dendritic cells (cluster 10: 0.86%), and

491 plasmacytoid dendritic cells (cluster 11: 0.57%). We noted that the cell sizes of the T cells and
492 B cells from clusters 3, 4 and 5, which were measured using a cell sorter, were smaller than
493 those of MSCs and macrophages from clusters 1, 2, and 8 (Additional file 1: Figure S19). We
494 confirmed that the cell sizes of CD4-positive T cells and CD79-positive B cells were smaller in
495 SVF via immunofluorescence observation (Additional file 1: Figure S19). These results show
496 that Quartz-Seq2 with flow-cytometry data is useful for defining respective cell clusters with cell
497 size information.

498 Subsequently, we investigated the gene expression of receptors and ligands in stromal
499 vascular fractions. The variety of receptors expressed in each cluster was similar (Additional
500 file 1: Figure S21). However, we found a wide variety of ligands expressed in clusters 1 and 8
501 (Additional file 1: Figure S21). It is known that MSCs secrete many paracrine mediators, which
502 have a therapeutic effect [29,30]. These results suggest that clusters 1 and 8 are MSCs, which
503 secretes many paracrine mediators.

504 We focused on two potential MSC clusters (1 and 8) because the heterogeneity of the
505 MSC population has been discussed in many papers [31,32]. By using Quartz-Seq2, clusters 1
506 and 8 had the *Cd31-*/*Cd34+*/*Cd45-* phenotype (Figure 8, Additional file 1: Figure S22). In a
507 previous study, qPCR-based single-cell transcript analysis of the *Cd31-*/*Cd34+*/*Cd45-*
508 population of SVF was reported. By analyzing 140 genes, the authors identified the
509 *Cd55+*/*Dpp4+*/*Cd31-*/*Cd34+*/*Cd45-* cell population and showed that administration of this
510 population was effective for normalizing diabetic wound healing in mice [31]. They identified 13
511 marker genes for the *Cd55+*/*Dpp4+*/*Cd31-*/*Cd34+*/*Cd45* population in mouse SVF. We
512 compared the expression of those 13 genes between clusters 1 and 8 (Additional file 1: Figure
513 S23). The results showed that almost all the genes were more highly expressed in cluster 1
514 than in cluster 8, suggesting that the cluster 1 population was similar to the
515 *Cd55+*/*Dpp4+*/*Cd31-*/*Cd34+*/*Cd45-* population. To further analyze the relationship between our
516 identified clusters and previously reported heterogeneity of the MSC population, we examined
517 the expression of typical MSC markers (*CD90*, *CD105, PDGFRa,* and *Sca-1*) [31,33] as well as
518 subpopulation specific markers (*Pou5f1*, *Nanog*, *Sox2*, *Tnnt2*, and *Myog*) [34,35]. *PDGFRa*
519 (*Pdgfra*) and *Sca1* were expressed in both clusters 1 and 8, whereas *Cd90* was expressed at a

520 relatively higher level in cluster 8 than in cluster 1, and *Cd105* was not strongly expressed in
521 either cluster. *Cd90* and *Cd105* were, however, not specific to these MSC clusters. Neither
522 pluripotent markers (*Pou5f1*, *Nanog*, and *Sox2*) nor skeletal and cardiomyogenic markers
523 (*Tnnt2* and *Myog*) were detected in either cluster (Additional file 1: Figure S22). Collectively,
524 our transcriptome analysis showed that the MSC population is divided into two clusters,
525 suggesting that there is less heterogeneity of MSC in the SVF than expected.

526 Next, we investigated the difference between the two MSC clusters in SVF. We detected
527 182 differentially expressed genes between clusters 1 and 8 (Additional file 1: Figure S24,
528 Additional file 5: Table S4). Cluster 8 was characterized by the enriched expression of genes
529 that encode extracellular matrix proteins, including collagens, *Hspg2*, and *Bgn*. By contrast,
530 cluster 1 was characterized by the expression of *IGFBPs* (*Igfbp4*, *Igfbp5*, *Igfbp6*), prostaglandin
531 endoperoxidase synthases (*Ptgs2*), and secreted factors *Fgf2* and Bmp2. Of note, the
532 expression of stem cell characteristic genes *Aldh1a3*, *Fgf2*, *Bmp2*, and *Tgfbr2* were identified
533 as important modules in cluster 1, suggesting that cluster 1 had more stem-like phenotypes
534 that secrete medicinal factors.

535 To leverage the power of the entire transcriptome analysis, we performed an enrichment
536 analysis of biological pathways using the 182 differentially expressed genes between the two
537 clusters (Figure 8e, Additional file 6: Table S5). Cluster 1 was characterized by elastic fiber
538 pathways and IGF transport pathways. Elastic fibers contribute various connective tissues and
539 are related to vascular function [36]. Growth factors including FGF2, BMP2, IGFBPs, and PGE2
540 regulate growth and differentiation [37]. In cluster 8, a tightly linked network of collagen
541 metabolism pathways was highly enriched. These results suggest that two MSC clusters of SVF
542 have different functions. Cluster 1 could be medicinal cell characterized by the expression of
543 growth and development-related genes. On the other hand, cluster 8 may be characterized by
544 production of extracellular matrix.

545 Taken together, our transcriptome analysis by Quart-seq2 successfully identified cell
546 populations that consisted of various types of both large and small cells, which were isolated
547 from *in vivo* tissue, and demonstrated that fresh SVF contains two closely related types of
548 MSCs that have distinct characteristics.

549 **Discussion**

550 The rate of conversion from initial reads to UMI counts was low, especially in high-throughput
551 single-cell RNA-seq. An increase in UMI counts assigned to each cell theoretically leads to the
552 detection of low-copy genes and the identification of cell-type-specific genes using statistical
553 tests. Therefore, in this study, we developed a novel high-throughput single-cell RNA-seq
554 method, Quartz-Seq2. We calculated the UMI conversion efficiency, which indicated how
555 effectively initial reads can be converted to UMI counts. The UMI conversion efficiency of
556 Quartz-Seq2 was higher than those of other single-cell RNA-seq methods (Additional file 1:
557 Figure S12). In other words, Quartz-Seq2 could detect more genes from limited fastq reads and
558 for a lower cost. By cell barcoding, Quartz-Seq2 can pool cDNA of up to 1,536 individual cells
559 into one mixture. Streamlined and simplified experimental processes of Quartz-Seq2 allowed us
560 to handle thousands of single cells within a few days. Quartz-Seq2 also showed high accuracy
561 and high reproducibility, leading to precise measurement of the transcriptome from single cells
562 (Figure 2d and e). We demonstrated Quartz-Seq2 analyses on mouse ES cells as an i*n vitro*
563 sample, and mouse SVF including MSC as an *in vivo* sample. Moreover, we decreased the
564 cDNA preparation cost per cell of Quartz-Seq2 by 97.6%-98.2% compared with that of
565 Quartz-Seq (Figure S8c). The total cost (cDNA preparation cost and sequence cost per cell) of
566 Quartz-Seq2 as a cell sorter based method approached that of a droplet-based method
567 (Additional file 1: Figure S8d). Furthermore, the use of evaporation-preventing oil might reduce
568 the cDNA preparation cost of Quartz-Seq2 by 75% [2].

569 We proposed that UMI conversion efficiency could be a useful variable for evaluating
570 performance for the further development of high-throughput single-cell RNA-seq methods with
571 shallow reads. The increase of initial sequence reads by additional sequencing does not cancel
572 out the low efficiency of UMI conversion at equal rate. For example, approximately 24,000 fastq
573 reads were converted to approximately 11,000 UMI counts in Quartz-Seq2, while Drop-seq
574 required approximately 169,000 fastq reads to generate the same UMI counts. At this condition,
575 the difference of UMI conversion efficiency was 2.5-fold but the difference of required fastq reads
576 to generate the same UMI counts was 7-fold. This is because UMI counts do not linearly
577 increase with an increase of initial sequence reads due to UMI filtering. Unfortunately, the rate of

578 increase of sequence throughput was lower than that of the processing ability for single cells. It
579 will thus continue to be important to utilize limited initial fastq reads for high-throughput
580 single-cell RNA-seq methods.

581 Quartz-Seq2 is based on the poly-A tagging, which is one of the strategies of
582 converting first-strand cDNA to amplified cDNA [19,38]. However, the poly-A tagging efficiency
583 itself has not been improved for single-cell RNA-seq. In this study, three molecular biological
584 improvements on Quartz-Seq2 contributed to the increase of amplified cDNA, which led to high
585 UMI conversion efficiency (Figure 2 and Additional file1: Figure S1). In addition, improvement of
586 poly-A tagging steps was most efficient to increase amplified cDNA for Quartz-Seq2 (up 360%,
587 Additional file 1: Figure S1). Several previous studies improved the efficiency of conversion from
588 an mRNA molecule to amplifiable cDNA, and showed that the increase of amplified cDNA is a
589 good guidepost to improve UMI counts or quantitative performance for single-cell RNA-seq
590 [3,14,15]. These results suggest that improved poly-A tagging was the most important point for
591 high UMI conversion efficiency of Quartz-Seq2.

592 Several improvements proposed in this study could contribute to the further
593 development of other single-cell RNA-seq methods, as follows. (1) We showed that a decrease
594 of enzyme concentration in RT solution led to decreases in technical error and cDNA preparation
595 cost. (2) We applied the Sequence–Levenshtein distance for the design of cell barcodes
596 containing RT primer sets. The use of primer sets designed in this study allows the user to
597 correct mutations of at most two nucleotides of cell barcode, including substitution, insertion, or
598 deletion; the correction capability of these primer sets is higher than that of barcode sets used in
599 previous studies [1,3]. Such correction of the cell barcode increased the average UMI count by
600 3%–5%. (3) We hope that the spin-down collection system developed in this study can be
601 applied to other cell sorter based single-cell RNA-seq methods [2,3,11,12]. (4) In Quartz-Seq2,
602 we improved the efficiency of poly-A tagging itself (Figure 2). Several single-cell RNA-seq
603 methods including Quartz-Seq were based on poly-A tagging [4,5,10,15,19,39]. Such
604 improvement may directly contribute to these methods having increased quantitative
605 performance.

606 We achieved a marked improvement in UMI conversion efficiency from initial reads to
607 UMI counts, allowing us to analyze 3- to 10-fold more single cells in limited sequence
608 experiments. However, it is difficult to sort more than 20,000 single cells using one cell-sorter
609 machine in a day. While there is greater scalability for cell sampling in droplet-based single-cell
610 RNA-seq methods than in cell sorter-based methods, these latter methods can utilize additional
611 information obtained in flow cytometry [40,41], which cannot be determined from transcriptome
612 data alone. These two types of method provide complementary approaches for investigating
613 complex biological phenomena. C1 Single-Cell Auto Prep System (Fluidigm) is another widely
614 used platform for single-cell RNA-seq methods [42]. CEL-seq2 shows high UMI conversion
615 efficiency, so it is a very convenient method for users of C1 platform as a single-cell RNA-seq
616 method based on UMI count [3]. Quartz-Seq2 cannot be performed with C1 platform, but it can
617 assimilate 1,536 cell barcodes in a cell sorter in a high-throughput manner. We think that both
618 methods can be effective as long as the most appropriate one is selected for each situation.
619 In this study, we showed that Quartz-Seq2 has advantages in gene detection and the
620 identification of biological pathways via high UMI conversion efficiency (Figures 4, 5, and 7).
621 Moreover, we analyzed thousands of single cells from all cell cycle phases within a cell type
622 (Figure 7). These specifications with Quarz-Seq2 allow us to perform the global classification of
623 genes with variable expression in a cell type into those whose expression varies in association
624 with the cell cycle or independently of it.
625 A previous study utilizing the FUCCI fluorescent reporter system reported that
626 competence to respond to specific differentiation signaling was limited to only an early or a late
627 window of the G1 phase in human ES cells [43]. In the future, combining Quartz-Seq2 and
628 FUCCI/FUCCI2 or other fluorescent reporter systems will lead to an understanding of the
629 global picture of differentiation dynamics on competence, response, transition, and
630 commitment because Quartz-Seq2 can analyze changes of cell state for thousands of cells.
631 In summary, Quartz-Seq2 can be used to detect continuous cell states because of the
632 large number of cells with which it deals and the high efficiency of use of initial sequence reads.
633 Quartz-Seq2 can facilitate investigation of the cell state within a cell type, such as gradient or
634 stochastic changes of the cell population in organism development and disease progression.

635 **Conclusions**

636 In this study, we developed a high-throughput single-cell RNA-seq method, Quartz-Seq2, which
637 can analyze cells numbering up to 1,536 that are pooled together in a single sample.
638 Quartz-Seq2 allows us to effectively utilize initial sequence reads from a next-generation
639 sequencer. The UMI conversion efficiency in Quartz-Seq2 ranged from 30% to 50%, which is
640 much higher than for other single-cell RNA-seq methods (5%–20%). This was caused by the
641 improvements in several molecular biological steps including poly-A tagging. The technical gene
642 expression variability of Quartz-Seq2 was sufficiently low, and that was close to the theoretical
643 variability of a Poisson distribution. As we showed in the analysis of SVF and the ES/PrE mixture,
644 cell types in the population were identified with marker genes and functional terms that
645 characterized each cell type. We identified two types of *Cd34*-positive MSC in SVF, namely,
646 those that express numerous transcription factor-coding and secreted protein-coding genes
647 specific to each. Quartz-Seq2 can also be used to provide continuous data on cell states
648 because of the large number of cells with which it deals and the high efficiency in the use of initial
649 sequence reads. Quartz-Seq2 should facilitate investigations of the cell state within a cell type,
650 such as gradient or stochastic changes of cell populations in organism development and disease
651 progression.
652
653
654
655
656
657
658
659
660
661
662
663

664 **Methods**

665

666 **Cell culture**

667 Mouse embryonic stem cells were cultured as described previously [15]. Briefly, 1.0 x $10^5$ cells
668 were seeded on a 60-mm dish coated with gelatin (0.1%). Cells were maintained in
669 GMEM-based medium containing 10% FBS and 1000 units/ml leukemia inhibitory factor
670 (Millipore ESGRO). The cell line used in this study was G6GRGFP, which was established in a
671 previous study [44]. To differentiate ES cells into primitive endoderm-like cells, 1.0 x $10^5$ cells
672 were seeded on a 60-mm dish coated with gelatin and cultured in GMEM-based medium
673 containing 10% FBS, 1000 units/ml LIF, and 100 mM dexamethasone for 72 h.

674

675 **Cell staining**

676 To identify dead or damaged cells, propidium iodide (PI) was added to the cell suspension (final
677 concentration 1–2 μg/ml). As an indicator of an undifferentiated state in a suspension containing
678 a mixture of cells, Calcein-AM was used. Suspensions for cells cultured under maintenance and
679 differentiation conditions were prepared independently, and cells in the maintenance condition
680 were treated with 1 μg/ml Calcein-AM for 10 min on ice. After washing with PBS, cell
681 suspensions of ES cells and PrE cells at the same concentration were mixed. Hoechst 33342
682 was used as an indicator of the DNA content in a cell. The procedures were performed as
683 described previously [15].

684

685 **Single-cell preparation for stromal vascular fraction**

686 These experiments were carried out in accordance with the protocol approved by the National
687 Institute of Advanced Industrial Science and Technology (AIST) Animal Care and Use
688 Committee and the RIKEN Animal Experiment Committee. Subcutaneous fat tissues from three-
689 to four-month-old ICR male mice (n=3 per sample, two biological replicate samples) were
690 minced into small pieces and incubated with 0.4 U/mL collagenase NB4G (Serva) at 37°C for 35
691 min in a shaking water bath. The digested solution was sequentially filtered through 100-μm and
692 40-μm cell strainers (Corning), followed by centrifugation at 250 × *g* for 5 min to remove mature

693 adipocytes. The pellet was treated with erythrocyte lysis buffer (BD Biosciences) and centrifuged
694 at 180 × *g* for 5 min. The nucleated cells were suspended in HBSS with 0.1% BSA, filtered
695 through a 20-μm cell strainer (pluriSelect), and then kept on ice (Cell solution A). The cell
696 aggregates that did not pass through the 20-μm strainer were further treated with Accutase
697 (Thermo Fisher Scientific) at 37°C for 15 min to dissociate them into single cells, centrifuged at
698 180 × *g* for 5 min, and suspended in HBSS with 0.1% BSA (Cell solution B). Cell solutions A and
699 B were mixed and again filtered through the 20-μm cell strainer, followed by centrifugation at 180
700 × *g* for 5 min. The pellet was resuspended with HBSS with 0.1% BSA, stained with PI, and used
701 for single-cell analysis.
702
703 **RNA preparation**
704 Total RNA was purified from cultured cells using Direct-zol RNA MiniPrep kit (Zymo Research)
705 with TRIzol RNA Isolation Reagents (Thermo). We measured the concentration of purified total
706 RNA using a NanoDrop 1000 Spectrophotometer (Thermo). We confirmed that the RNA integrity
707 number of total RNA was over 9.5 using an Agilent RNA 6000 Nano Kit (Agilent). For
708 high-throughput single-cell RNA-seq, we prepared total RNA from a single cell with ERCC
709 spike-in mix I. First, we diluted the ERCC spike mix I by tenfold. We then added 6 μL of 1:10
710 diluted ERCC spike-in mix I per 10 μg of total RNA. We used diluted 10 pg of total RNA with
711 ERCC spike mix I for the technical validation of Quartz-Seq2.
712
713 **Bulk RNA-seq methods for populations of cells**
714 We prepared sequence library DNA with 1 μg of total RNA using NEBNext Poly(A) mRNA
715 Magnetic Isolation Module and NEBNext Ultra Directional RNA Library Prep Kit. The total RNA
716 did not contain ERCC spin-in mix I. In addition, we used SuperScript III instead of ProtoScript in
717 the reverse-transcription step and KAPA HiFi DNA polymerase instead of NEBNext High-Fidelity
718 PCR DNA polymerase in the PCR step. The resulting sequence library DNA was analyzed by
719 HiSeq2500.
720
721 **Design of cell barcodes**

722 The selection of 384 or 1,536 sequences for v3.1 and v3.2 barcode primer sets was performed
723 as described below. First, 1,582 or 4,714 candidate sequences were created using the
724 DNABarcodes package of R Bioconductor for the v3.1 set with 14-mer and the v3.2 set with
725 15-mer, respectively (version: 1.0.0). To reduce the loss of reads converted into UMI counts, we
726 applied the Sequence–Levenshtein distance as an edit distance in order to maximize the ability
727 to correct errors that occur during the synthesis of oligonucleotides or sequencing [22]. The
728 minimum distance between any two sequences was controlled to 5, leading to the correction of a
729 maximum of two errors of substitution, insertion, or deletion. As the base composition of the
730 created sequences was not uniform, we selected 384 or 1,536 sequences from among 1,582 or
731 4,714 created sequences so that the variance of base composition decreased. These sequences
732 are listed in Additional file 3: Table S2.
733
734 **Single-cell collection using flow cytometry**
735 Stained cells were analyzed using flow cytometry SH800 (Sony) or MoFlo Astrios EQ (Beckman
736 Coulter). For SH800, we used 130-μm microfluidic sorting chips. For MoFlo Astrios EQ, we used
737 100-μm nozzle sizes. Each cell sorter was equipped with a custom-made splash-guard to
738 prevent contamination from unexpected droplets between the target well and neighboring wells.
739 We used two sets of RT primer for Quartz-Seq2. The set of v3.1 RT primers has 384 kinds of
740 unique cell barcodes, with a length of 14 nucleotides (OPC purification, FASMAC). The set of
741 v3.2 RT primers has 1,536 kinds of unique cell barcodes, with a length of 15 nucleotides (OPC
742 purification, Sigma). The set of v3.1 RT primers corresponds to one set of the 384-well PCR
743 plate with lysis buffer, the wells of which have unique barcodes. The set of v3.2 RT primers
744 corresponds to four sets of the 384-well PCR plate with lysis buffer. The RT primer position in the
745 384-well plate and the sequence were as described in Additional file 3: Table S2. Single cells
746 were isolated in the 384-well PCR plate with 1 μL of lysis buffer (0.1111 μM respective RT
747 primers, 0.12 mM dNTP mix, 0.3% NP-40, 1 unit/μL RNasin plus) containing ERCC spike mix I.
748 During single-cell sorting, the 384-well PCR plate was kept on a 384 aluminum stand at 4ºC. For
749 Moflo Astrios EQ, we used G5498B-060 Insert 384 Eppendorf twin.tec PCR as a 384 aluminum
750 stand (Agilent). For SH800, we used an SH800 384 aluminum stand (Sony). Immediately after

751 the cell collection, the plate was temporarily sealed with LightCycler 480 Sealing Foil (Roche)
752 and the sealed 384-well PCR plate was centrifuged at 10,000 g and 4ºC for 1 min using TOMY
753 MX307, equipped with a Rack-in-Rotor and centrifugation rack PCR96-02. These steps were
754 very important to collect the droplet with a single cell in lysis buffer in an efficient manner. By
755 altering the volume of lysis buffer from 0.4 µL (as described in the original Quartz-Seq paper) to
756 1 µL (Quartz-Seq2), bubbling of lysis buffer was not required before single-cell sorting and the
757 lysis buffer could easily be handled. We then peeled open the temporary seal and re-sealed it
758 with Agilent PlateLoc Thermal Microplate Sealer (Agilent). We agitated the plate at 2,600 rpm
759 and 4ºC for 1 min using ThermoMixer C (Eppendorf), after which we centrifuged the plate again.
760 The resulting 384-well plate was then immediately cryopreserved at −80ºC and maintained
761 under such conditions until subsequent reverse transcription for cell barcoding. After
762 cryopreservation, we performed subsequent whole-transcript amplification using the
763 cryopreserved 384-well PCR plate within a few months.
764
765 **Whole-transcript amplification of Quartz-Seq2**
766 Cryopreserved 384-well plates with single-cell lysate were centrifuged at 10,000 g and 4ºC for 1
767 min. Subsequently, we denatured total RNA in each 384 plate at 70ºC for 90 s and hybridized the
768 RT primer to poly-adenylated RNA at 35ºC for 15 s using the C1000/S1000 thermal cycler. The
769 resulting plates were again centrifuged at 10,000 g and 4ºC for 1 min. Next, the plates were
770 placed on the 384 aluminum plate at 0ºC. We peeled away the seal and added 1 µL of RT
771 premix (2x Thermopol buffer, 5 units/µL SuperScript III, 0.55 units/µL RNasin plus) to 1 µL of
772 lysis buffer for each well using a Mantis microfluidic dispensing system (Formulatrix) or a 384
773 Transfer Plate system (1859-384S, Watson). The above RT solution was used for the RT25
774 condition. For the RT100 condition, we used the following RT solution: 2x Thermopol buffer, 20
775 units/µL SuperScript III, and 2.2 units/µL RNasin plus. We sealed the plates again and agitated
776 them at 2,600 rpm and 4ºC for 1 min. The plates were then centrifuged at 10,000 g and 4ºC for 1
777 min. We then performed reverse transcription at 35ºC for 5 min and 50ºC for 50 min. The reverse
778 transcription was stopped at 70ºC for 15 min. Then, the plates were placed on a prechilled
779 aluminum block, after which we peeled off their seals. Subsequently, we turned the plates upside

780 down on the assembled collector type A or type B (supplemental figure). We mainly used type A.
781 We centrifuged the plates with an assemble collector at 3,010 g and 4ºC for 3 min with
782 swing-bucket rotors. Subsequently, we collected the cDNA solution into a disposable reservoir.
783 Typically, we obtained 650–700 μL of cDNA solution from one 384-well PCR plate. We purified
784 and concentrated the cDNA solution using the DNA Clean & Concentrator™-5 kit (Zymo
785 Research). We used three purification columns for one 384-well PCR plate in the case of the
786 v3.1 RT primer system (384-cell barcode). Purified cDNA was extracted into 20 μL of
787 nuclease-free water from one column purification and transferred into an eight-linked PCR tube
788 (TaKaRa). The PCR tubes were placed on an aluminum PCR stand at 0ºC. We added 25 μL of
789 TdT solution [1x Thermopol buffer, 2.4 mM dATP, 0.0384 units/μL RNase H (Invitrogen), 26.88
790 units/μL terminal transferase (Roche)] into 20 μL of extracted cDNA using a pipette at 0ºC. The
791 resulting 45 μL of TdT solution was mixed with a pipette at 0ºC or ThermoMixer at 2,000 g and
792 0ºC for 1 min. Immediately thereafter, the PCR tubes were centrifuged at 10,000 g and 0ºC for 1
793 min. We used a C1000/S1000 thermal cycler equipped with the 96-Deep Well Reaction Module
794 for the following steps. The PCR tubes were placed on the block of the thermal cycler, which had
795 been prechilled to 0ºC. We then performed a poly-A tailing reaction at 37ºC for 75 s. The solution
796 was inactivated at 65ºC for 10 min. The PCR tubes were placed on an aluminum PCR stand at
797 0ºC. We then dispensed approximately 11 μL of solution into four wells from 45 μL of TdT
798 solution. We added 46.16 μL of PCR I premix (1.08492x MightyAmp Buffer version 2, 0.06932
799 μM Tagging primer, 0.05415 units/μL MightyAmp DNA polymerase) to 11 μL of TdT solution for
800 the respective wells of the PCR tube. We performed gentle inversion mixing on the resulting
801 solution in the PCR tube. The tubes were then centrifuged at 10,000 g and 4ºC for 1 min.
802 Subsequently, the solution was mixed with ThermoMixer at 2,000 rpm and 4ºC for 2 min. Then,
803 we spun down the tube again. Next, we denatured the solution at 98ºC for 130 s and hybridized
804 Tagging primer to poly-A-tailed cDNA at 40ºC for 1 min. After that, we performed the “Increment
805 step” by heating to 68ºC at 0.2ºC every second and performed second-strand synthesis at 68ºC
806 for 5 min. The tubes were placed on an aluminum PCR stand at 0ºC. We added 50.232 μL of
807 PCR II premix (0.99697x MightyAmp Buffer version.2, 1.8952 μM gM primer) to 56.16 μL of PCR
808 I solution. We performed gentle inversion mixing on the resulting solution in the PCR tube. The

809 tubes were then centrifuged at 10,000 g and 4ºC for 1 min. Subsequently, the solution was
810 mixed with ThermoMixer at 2,000 rpm and 4ºC for 2 min, after which we spun down the tube
811 again. We then placed it on the block of the thermal cycler at 68ºC. Subsequently, we amplified
812 the cDNA for 11 cycles under the following conditions: 98ºC for 10 s, 65ºC for 15 s, and 68ºC 5
813 min. We then incubated the tube at 68ºC for an additional 5 min. Finally, we transferred all of the
814 PCR solution, derived from one 384-well PCR plate, to a 50-mL Polypropylene Centrifuge Tube
815 (Watson). Typically, we obtained approximately 1.2 mL of PCR solution per 384-well PCR plate.
816 We added 32 μL of 3 M sodium acetate (pH 5.2) and 6420 μL PB-Buffer (Qiagen) to the PCR
817 solution. The mixture was then purified using a MinElute Spin Column (Qiagen). Purified cDNA
818 was extracted into 40 μL of nuclease-free water. We additionally purified the cDNA with 32 μL of
819 Ampure XP beads. Finally, we obtained 32 μL of purified cDNA. We checked the length
820 distribution of amplified cDNA with an Agilent High Sensitivity DNA Kit (Agilent). The typical
821 average size of the amplified cDNA in Quartz-Seq2 was approximately 1,400 bp (Additional file
822 1: Figure S2c). Primer sequences are listed in Additional file 3: Table S2.
823 In the case of the usage of the v3.2 RT primer in Quartz-Seq2, we modified the above
824 steps as follows. After reverse transcription, we collected cDNA solution into a disposable
825 reservoir from four sets of 384-well plates, which corresponded to 1,536 wells. We purified and
826 concentrated the cDNA solution using eight purification columns for four 384-well PCR plates in
827 the case of the v3.2 RT primer system. In the PCR step, we amplified cDNA for nine cycles with
828 the following conditions: 98ºC for 10 s, 65ºC for 15 s, and 68ºC for 5 min. Finally, we transferred
829 all of the PCR solution derived from four 384-well plates to a 50-mL Polypropylene Centrifuge
830 Tube (Watson). Typically, we obtained approximately 3.5 mL of PCR solution per four 384-well
831 PCR plates. We added 88 μL of 3 M sodium acetate (pH 5.2) and 17.6 mL of PB-Buffer (Qiagen)
832 to the PCR solution. The mixture was purified using the MinElute Spin Column (Qiagen).
833 Subsequently, cDNA was again purified using Ampure XP magnetic beads.
834 For the Quartz-Seq1-like reaction, we performed the following procedure in
835 accordance with our previous study. We added 1 μL of RT premix (2x PCR buffer, 5 units/μL
836 SuperScript III, 0.55 units/μL RNasin plus) to 1 μL of lysis buffer. We then performed reverse
837 transcription at 35ºC for 5 min and 45ºC for 20 min. This reverse transcription was stopped at

838 70ºC for 15 min. We added 5 μL of ExoIB solution (1.6x Exonuclease I buffer, 3.2x PCR buffer,
839 16 mM DTT) and 20 μL of TdT solution [1x PCR buffer, 3 mM dATP, 0.0384 units/μL RNase H
840 (Invitrogen), 33.6 units/μL terminal transferase (Roche)] into 20 μL of extracted cDNA using a
841 pipette at 0ºC. The PCR tubes were placed on the block of the thermal cycler that had been
842 prechilled to 0ºC. We performed a poly-A tailing reaction at 37ºC for 75 s. We then denatured the
843 solution at 98ºC for 130 s and hybridized Tagging primer to poly-A-tailed cDNA at 40ºC for 1 min.
844 After that, we performed second-strand synthesis at 68ºC for 5 min. Subsequently, we amplified
845 the cDNA via a PCR reaction for 12 cycles.
846
847 **Preparation of truncated sequence adaptor**
848 The truncated sequence adaptor was composed of an rYshapeP5 primer (HPLC-purified) and
849 rYshapeP7LT primers (HPLC-purified), which had a TruSeqLT-compatible pool barcode. We
850 prepared 100 μM respective primers with adaptor buffer (10 mM Tris-HCl pH7.8, 0.1 mM EDTA
851 pH8.0, 50 mM NaCl). We added 5 μL of 100 μM rYshapeP5 primer and rYshapeP7LTxx primer
852 into a single PCR tube. We denatured the solution at 90ºC for 90 s. After that, we achieved
853 annealing by cooling to 10ºC by 0.5ºC every 30 s and then maintaining the sample at 4ºC. We
854 then placed the tube on an aluminum PCR stand at 0ºC. Subsequently, we added adaptor buffer,
855 which was prechilled at 0ºC, to 10 μL of 50 μM truncated adaptor. Finally, we obtained about 50
856 μL of 10 μM truncated adaptor. We cryopreserved 1 μL of 10 μM truncated adaptor in a PCR
857 tube at −80ºC until usage in the adaptor ligation step. Primer sequences are listed in Additional
858 file 3: Table S2.
859
860 **Sequence library preparation of Quartz-Seq2**
861 We added 130 μL of nuclease-free water including 5–10 ng of amplified cDNA into a Crimp-Cap
862 microTUBE with AFA Fiber. We then performed cDNA fragmentation using an LE220
863 Focused-ultrasonicator (Covaris) under the following conditions: duty factor 15%, peak incident
864 power 450 W, cycles per burst 200, and treatment time 80 s. We purified and concentrated the
865 cDNA solution using the DNA Clean & Concentrator™-5 kit. Purified cDNA was extracted into 10

866 μL of nuclease-free water from one column purification and transferred into an eight-linked PCR
867 tube (TaKaRa).
868 We then added 2 μL of End-Repair premix [1.4 μL of End repair & A-tailing buffer and
869 0.6 μL of End repair & A-tailing Enzyme (KAPA Biosystems)] to 10 μL of fragmented cDNA
870 solution. Subsequently, we mixed the solution by pipetting on an aluminum PCR stand at 0ºC.
871 The PCR tubes were placed on the block of the thermal cycler, which had been prechilled to
872 20ºC. We then incubated the tubes at 37ºC for 60 min and 65ºC for 30 min. After this, we added
873 2 μL of adaptor buffer (1.5 μM truncated adaptor, 10 mM Tris-HCl pH7.8, 0.1 mM EDTA pH8.0,
874 50 mM NaCl) and 8 μL of ligation premix [6 μL of ligation buffer, 2 μL of DNA ligase (KAPA
875 Biosystems)] at 4ºC. The 22 μL of ligation solution was well mixed by pipetting at 4ºC. Then, we
876 performed adaptor ligation at 20ºC for 15 min. After ligation, we added 18 μL of Ampure XP
877 beads to 22 μL of adaptor ligation solution and mixed them well. Adaptor-ligated cDNA was
878 extracted into 20 μL of nuclease-free water. We added 32 μL of PCR premix [25 μL of 2xKAPA
879 HiFi ready mix, 1.75 μL of 10 μM TPC2 primer (HPLC-purified), 10 μM P5-gMac hybrid primer
880 (HPLC-purified)] to 18 μL of adaptor-ligated cDNA. We denatured the solution at 98ºC for 45 s.
881 Subsequently, we amplified cDNA for eight cycles under the following conditions: 98ºC for 15 s,
882 60ºC for 30 s, and 72ºC for 1 min. Finally, we additionally incubated the tube at 72ºC for 5 min.
883 We added 40 μL of Ampure XP beads to 50 μL of PCR solution. Purified
884 sequence-library DNA was eluted into 20–30 μL of nuclease-free water. We checked the DNA
885 concentration and DNA size of sequence library DNA using the Agilent High Sensitivity DNA Kit
886 (Agilent) and QuantiFluor® dsDNA System (Promega). We also prepared sequence library DNA
887 with Tn5 transposase, in accordance with a modified version of a procedure used in a previous
888 study [6]. Specifically, the modifications were as follows. We used 0.75 ng of amplified cDNA for
889 the Nextera XT library preparation kit. We amplified sequence library DNA with the P5-gMac
890 hybrid primer and the Nextera XT primer, which has the P7 sequence.
891
892 **Deep sequencing for Quartz-Seq2**
893 We analyzed the sequence library DNA from Quartz-Seq2 using NextSeq500 (Illumina) and
894 HiSeq2500 (Illumina). For the Read1 sequence, we used a custom sequence primer named

895 Read1DropQuartz primer (HPLC-purified). In the case of the v3.1 RT primer, sequence
896 specification was as follows (Read1: 22 cycles, Index1: 6 cycles, Read2: 64–118 cycles). In the
897 case of the v3.2 RT primer, sequence specification was as follows (Read1: 23 cycles, Index1: 6
898 cycles, Read2: 63 cycles). When Read1 length was within 64 nt we mainly used the NextSeq
899 500/550 High Output v2 Kit (75 cycles), which can be used for sequencing up to 92 nt. For long
900 sequences (over 64 nt), we analyzed sequence library DNA using the HiSeq Rapid SBS Kit v2.
901 Sequence analysis with HiSeq2500 was supported by the Genomic Network Analysis Support
902 facility (GeNAS) in RIKEN.
903
904 **Amplification-free single-cell qPCR analysis**
905 Amplification-free single-cell qPCR was performed in accordance with our previous study with
906 the following modifications [15]. We collected a single cell into 1 μL of lysis buffer (2.5 μM
907 random hexamer, 1 mM dNTP mix, 0.3% NP40, 2 units/μL RNasin plus) of a 384-well PCR plate
908 (Eppendorf) using SH800. The resulting 384-well PCR plate was cryopreserved at −80ºC. We
909 denatured total RNA in the 384-well PCR plate at 70ºC for 1.5 min using a C1000/S1000 thermal
910 cycler and hybridized the random primer to RNA at 0ºC for 2 min. We added 1 μL of
911 reverse-transcription solution (2x SSIV buffer, 10 mM DTT, 2 units/μL RNasin plus, 20 units/μL
912 SuperScript IV) to the lysis buffer. Subsequently, we performed reverse transcription at 23ºC for
913 10 min and 50ºC for 10 min. The reverse transcription was stopped at 80ºC for 10 min. The
914 resulting solution was diluted with qPCR solution (10 mM Tris-HCl pH 8.0, 0.05% Tween-20).
915 The obtained diluted solution was then used for qPCR detection with QuantiTect SYBR Green
916 PCR Master Mix and the LightCycler480 system. For primer sets for each gene, see Additional
917 file 3: Table S2.
918
919 **Drop-seq experiments and data analysis**
920 Drop-seq was performed as reported previously [6] and in line with an online protocol
921 (http://mccarrolllab.com/dropseq/), but with the following modifications: flow rates for oil and
922 aqueous suspensions were 14,000 μl/h and 4,000 μl/h, respectively. The diameter of droplets
923 was 95–100 μm. Microfluidic devices were fabricated by Fluidware Technologies (Japan). The

924 lot number of barcoded beads was 051415 (ChemGenes). Data analysis for Drop-seq was
925 performed as described online (http://mccarrolllab.com/dropseq/). The versions of the software
926 and databases were as follows: STAR: v2.5.1b; mouse genome: mm10; genome annotation:
927 gencode GRCm38.p4 vM9; and Drop-seq tools: v1.11.
928
929 **Quartz-Seq2 read alignment and generation of digital expression data**
930 The structure of the sequence library and data processing was designed based on those of
931 Drop-seq ([6] and online as referenced above). BCL files generated by Illumina NextSeq500
932 were converted to fastq files by bcl2fastq2 (v2.17.1.14) with demultiplexing pool barcodes. The
933 --mask-short-adapter-reads parameter was set to 20. If needed, fastq reads were randomly
934 downsampled by seqtk software (version: sgdp). The last two bases of Read2, the sequence
935 quality of which was relatively low, were removed by FASTX-Toolkit (version: 0.0.14). Fastq files
936 for Read1 and Read2 were converted to a bam file by FastqToSam of Picard tools (version:
937 1.134). Extracting cell barcodes and UMI (equal to molecular barcode) and filtering out reads
938 with low barcode quality were performed using Drop-seq tools (version: 1.11). The resulting bam
939 files were re-converted to fastq files by SamToFastq of Picard tools, and mapped to the mouse
940 genome (mm10) using STAR (version: 2.5.1b). After sorting the resulting bam files by SortSam
941 of Picard tools, the unaligned bam and aligned bam were merged by MergeBamAlignment of
942 Picard tools. Then, gene names were assigned to each record using TagReadWithGeneExon of
943 Drop-seq tools and gtf file (version: gencode GRCm38.p4 vM9). For the correction of errors of
944 cell barcodes considering the Sequence–Levenshtein distance, a custom-made python program
945 was used, which enabled the correction of up to two errors of substitution, insertion, or deletion.
946 This program used python2 (version: 2.7.11+), PypeR (version: 1.1.2), R (version: 3.2.3),
947 Bioconductor (version: 3.2), and Bioconductor package DNABarcodes (version: 1.0.0). Finally,
948 the UMI for each gene for each cell was counted using DigitalExpression of Drop-seq tools,
949 which generated the digital expression matrix. To generate a non-UMI-filtered matrix, a
950 custom-made python program that counts reads for each gene for each cell was used.
951
952 **Dimensionality reduction, clustering, and term analysis**

953 Cells with low detected gene counts were removed for further analysis (Quartz-Seq2 on ES/PrE
954 mixture: 4,000 genes; Quartz-Seq2 on SVF: 500 genes). Total counts of each cell were
955 normalized to 10,000 or the mean of total UMI counts for cells. UMI counts had 1 added to them
956 and were then log-transformed (natural logarithm), after which they were scaled to have mean
957 and variance for each gene of 0 and 1, respectively. For PCA, UMI counts for all detected genes
958 (for ES/PrE mixture) or genes with highly variable expression (for SVF) were used. For t-SNE,
959 the top 10 to 40 principal components of matrices produced by PCA were used. For clustering,
960 the DBSCAN algorithm was used. The values of the parameter epsilon were 0.69 for
961 Quartz-Seq2 on the 4,500 mouse ES/PrE mixture, 5 for Quartz-Seq2 on the 384 mouse ES/PrE
962 mixture, 3 for Drop-seq on the 500 mouse ES/PrE mixture, and 2.2 for SVF analysis.
963 Significantly enriched GO terms with the top principal components were calculated using the
964 GO-PCA package [45].
965
966 **Identification of differentially expressed genes for each cluster**
967 Marker genes for each cluster were identified based on a generalized linear model. The
968 difference in deviance between two models, in which the gene was or was not differentially
969 expressed between two clusters, was calculated for the genes. To filter out noise, pseudocount 1
970 was added to the averaged gene expression in clusters and only genes with fold change of 2 or
971 more between two clusters were further analyzed. P-values were calculated as 1 − cumulative
972 density function of a chi-squared continuous random variable for difference in deviance. After
973 corrections for multiple testing, genes with FDR of less than 0.05 were identified as differentially
974 expressed genes for the cluster. For comparison between differentially expressed genes
975 identified by scRNA-seq methods and those identified by bulk RNA-seq, this pseudocount was
976 not added.
977
978 **Identification of cell cycle-associated genes and cell cycle-phase independent variable**
979 **genes**
980 To identify genes for which the expression changes depending on the phase of the cell cycle, we
981 used the intensity of Hoechst 33342 staining measured using a cell sorter. First, cells were

982 discretized into 40 equal-sized buckets based on the rank of Hoechst 33342 staining intensity.
983 Then, the CV of averaged UMI counts for a gene in each bin was calculated. After z-scaling of
984 this, genes with high z-scores were identified. To identify genes whose expression fluctuates in a
985 manner not dependent on the cell cycle phase, we calculated the CV of UMI counts for a gene in
986 each cell and the CV of averaged UMI counts for a gene in each bin. After z-scaling of such data,
987 the genes of which difference between two scaled CV was large were identified as cell
988 cycle-phase independent variable genes.
989
990 **Enrichment analysis on pathway and Gene Ontology (GO) terms**
991 Pathways that were particularly enriched for the differentially expressed genes were calculated
992 using the ReactomePA package of R Bioconductor (version: 1.14.4, [46]) and Metascape
993 (http://metascape.org/ [47]). The cut-off parameter for the q value was 0.05. Terms that were
994 enriched for genes with highly variable expression were calculated using DAVID, the Database
995 for Annotation, Visualization and Integrated Discovery (version: 6.8, [48,49]). Ontology used for
996 calculation was GOTERM_BP_FAT, GOTERM_MF_FAT, and GOTERM_CC_FAT. The terms
997 with FDR < 0.05 were identified as enriched terms.
998
999 **Data resources**
1000 Raw and processed data files for Quartz-Seq2 and Drop-seq experiments are available under
1001 GEO: GSE99866 (https://www.ncbi.nlm.nih.gov/geo/query/acc.cgi?acc=GSE99866) for
1002 single-cell RNA-seq data and DRA002954 for bulk-RNA-seq data.
1003
1004
1005
1006
1007
1008
1009
1010

1011 **List of abbreviations**

1012

1013 UMI: unique molecular identifier

1014 PCR: polymerase chain reaction

1015 SCC: Spearman's rank correlation coefficient

1016 CV: coefficient of variation

1017 ES cell: embryonic stem cell

1018 PrE cell: primitive endoderm cell

1019 SVF: stromal vascular fraction

1020 RT: reverse-transcription

1021 Dex: dexamethasone

1022 PCA: principal component analysis

1023 MSC: mesenchymal stem cell

1024 TdT: terminal deoxynucleotidyl transferase

1025 GO: Gene Ontology

1026 FDR: false discovery rate

1027 t-SNE: t-distributed stochastic neighbor embedding

1028 nt: nucleotide

1029 bp: base pair

1030 SSC: side scatter

1031

1032

1033

1034

1035

1036

1037

1038

1039

1040 **Declarations**

1041

1042 **Ethics approval and consent to participate**

1043 Not applicable.

1044

1045 **Consent for publication**

1046 Not applicable.

1047

1048 **Availability of data and material**

1049 The data have been deposited under GEO accession number GSE99866 and DRA accession

1050 number: DRA002954.

1051

1052 **Competing interests**

1053 The authors declare that they have no competing interests.

1054

1055 **Funding**

1056 This work was supported by the Projects for Technological Development, Research Center

1057 Network for Realization of Regenerative Medicine by Japan, the Japan Agency for Medical

1058 Research and Development (AMED), and the Japan Science and Technology Agency (JST).

1059 The sequence analyses of bulk RNA-seq were supported by MEXT KAKENHI (No. 221S0002)

1060 and JSPS KAKENHI Grant Number JP24651218 and JSPS KAKENHI Grant number

1061 JP15K16329. The sequence operations of Quartz-Seq2 using HiSeq2500 were supported by the

1062 Platform Project for Supporting Drug Discovery and Life Science Research (Platform for Drug

1063 Discovery, Informatics, and Structural Life Science) from AMED.

1064

1065 **Author's contributions**

1066 YS, HD and IN designed the study. YS designed and performed experiments of single-cell

1067 RNA-seq. HD designed and performed data analysis. HT and AK designed and performed

1068 experiments of mouse stromal vascular fraction. ME assisted the experiments. TH assisted the

development of spin-down collection system. YS, HD, HT, AK and IN wrote the manuscript. All authors read and approved the final manuscript.

**Acknowledgements**

We greatly appreciate the Drop-seq team's useful comments about our technical introduction to Drop-seq. We thank Mr. Akihiro Matsushima and Mr. Manabu Ishii for their assistance with the infrastructure for the data analysis. We appreciate Dr. Christoph Ziegenhain and Dr. Wolfgang Enard for giving us their quantitative data from single-cell RNA-seq methods. We thank Dr. Yutaka Suzuki for his assistance with the bulk RNA-seq. We are grateful to Dr. Mika Yoshimura and Dr. Haruka Ozaki (RIKEN) for their assistance with the bulk RNA-seq analysis. Our thanks also go to Sony's cell sorter team for specially customizing the 384-well sorting mode of the SH800.

1098 **References**

1099

1100 1. Zheng GXY, Terry JM, Belgrader P, Ryvkin P, Bent ZW, Wilson R, et al. Massively parallel
1101 digital transcriptional profiling of single cells. Nat Commun. 2017;8:14049.

1102 2. Muraro MJ, Dharmadhikari G, Grün D, Groen N, Dielen T, Jansen E, et al. A Single-Cell
1103 Transcriptome Atlas of the Human Pancreas. Cell Syst. 2016;3:385–394.e3.

1104 3. Hashimshony T, Senderovich N, Avital G, Klochendler A, de Leeuw Y, Anavy L, et al.
1105 CEL-Seq2: sensitive highly-multiplexed single-cell RNA-Seq. Genome Biol. 2016;17:892.

1106 4. Fan X, Zhang X, Wu X, Guo H, Hu Y, Tang F, et al. Single-cell RNA-seq transcriptome
1107 analysis of linear and circular RNAs in mouse preimplantation embryos. Genome Biol.
1108 2015;16:236.

1109 5. Nakamura T, Yabuta Y, Okamoto I, Aramaki S, Yokobayashi S, Kurimoto K, et al. SC3-seq: a
1110 method for highly parallel and quantitative measurement of single-cell gene expression. Nucleic
1111 Acids Res. 2015;43:e60–0.

1112 6. Macosko EZ, Basu A, Satija R, Nemesh J, Shekhar K, Goldman M, et al. Highly Parallel
1113 Genome-wide Expression Profiling of Individual Cells Using Nanoliter Droplets. Cell.
1114 2015;161:1202–14.

1115 7. Klein AM, Mazutis L, Akartuna I, Tallapragada N, Veres A, Li V, et al. Droplet Barcoding for
1116 Single-Cell Transcriptomics Applied to Embryonic Stem Cells. Cell. 2015;161:1187–201.

1117 8. Fan HC, Fu GK, Fodor SPA. Combinatorial labeling of single cells for gene expression
1118 cytometry. Science. 2015;347:1258367–7.

1119 9. Bose S, Wan Z, Carr A, Rizvi A, Vieira G, Pe'er D, et al. Scalable microfluidics for single-cell
1120 RNA printing and sequencing. Genome Biol. 2015;16:120.

1121 10. Streets AM, Zhang X, Cao C, Pang Y, Wu X, Xiong L, et al. Microfluidic single-cell
1122 whole-transcriptome sequencing. Proc. Natl. Acad. Sci. 2014;111:7048–53.

1123 11. Jaitin DA, Kenigsberg E, Keren-Shaul H, Elefant N, Paul F, Zaretsky I, et al. Massively
1124 Parallel Single-Cell RNA-Seq for Marker-Free Decomposition of Tissues into Cell Types.
1125 Science. 2014;343:776–9.

1126 12. Soumillon M, Cacchiarelli D, Semrau S, van Oudenaarden A, Mikkelsen TS. Characterization
1127 of directed differentiation by high-throughput single-cell RNA-Seq. 2014.

1128 13. Islam S, Zeisel A, Joost S, La Manno G, Zajac P, Kasper M, et al. Quantitative single-cell
1129 RNA-seq with unique molecular identifiers. Nat. Methods. 2013;11:163–6.

1130 14. Picelli S, Björklund ÅK, Faridani OR, Sagasser S, Winberg G, Sandberg R. Smart-seq2 for
1131 sensitive full-length transcriptome profiling in single cells. Nat. Methods. 2013;10:1096–8.

1132 15. Sasagawa Y, Nikaido I, Hayashi T, Danno H, Uno KD, Imai T, et al. Quartz-Seq: a highly
1133 reproducible and sensitive single-cell RNA sequencing method, reveals non-genetic
1134 gene-expression heterogeneity. Genome Biol. 2013;14:R31.

1135 16. Hashimshony T, Wagner F, Sher N, Yanai I. CEL-Seq: Single-Cell RNA-Seq by Multiplexed
1136 Linear Amplification. Cell Rep. 2012;2:666–73.

1137 17. Ramsköld D, Luo S, Wang Y-C, Li R, Deng Q, Faridani OR, et al. Full-length mRNA-Seq
1138 from single-cell levels of RNA and individual circulating tumor cells. Nat. Biotechnol.
1139 2012;30:777–82.

1140 18. Islam S, Kjallquist U, Moliner A, Zajac P, Fan JB, Lonnerberg P, et al. Characterization of the
1141 single-cell transcriptional landscape by highly multiplex RNA-seq. Genome Res. 2011;21:1160–
1142 7.

1143 19. Tang F, Barbacioru C, Wang Y, Nordman E, Lee C, Xu N, et al. mRNA-Seq
1144 whole-transcriptome analysis of a single cell. Nat. Methods. 2009;6:377–82.

1145 20. Grün D, Kester L, van Oudenaarden A. Validation of noise models for single-cell
1146 transcriptomics. Nat. Methods. 2014;11:637–40.

1147 21. Ziegenhain C, Vieth B, Parekh S, Reinius B, Guillaumet-Adkins A, Smets M, et al.
1148 Comparative Analysis of Single-Cell RNA Sequencing Methods. Mol. Cell. 2017;65:631–4.

1149 22. Buschmann T. DNABarcodes: an R package for the systematic construction of DNA sample
1150 tags. Bioinformatics. 2017;:btw759.

1151 23. Ilicic T, Kim JK, Kolodziejczyk AA, Bagger FO, McCarthy DJ, Marioni JC, et al. Classification
1152 of low quality cells from single-cell RNA-seq data. Genome Biol. 2016;17:57.

1153 24. Zalzman M, Falco G, Sharova LV, Nishiyama A, Thomas M, Lee S-L, et al. Zscan4 regulates
1154 telomere elongation and genomic stability in ES cells. Nature. 2010;464:858–63.

1155 25. Pak J, Lee JH, Park KS, Park M, Kang L-W, Lee SH. Current use of autologous adipose
1156 tissue-derived stromal vascular fraction cells for orthopedic applications. J. Biomed. Sci.
1157 2017;24:1496.

1158 26. Trounson A, McDonald C. Stem Cell Therapies in Clinical Trials: Progress and Challenges.
1159 Cell Stem Cell. 2015;17:11–22.

1160 27. Baer PC, Geiger H. Adipose-Derived Mesenchymal Stromal/Stem Cells: Tissue Localization,
1161 Characterization, and Heterogeneity. Stem Cells Int. 2012;2012:1–11.

1162 28. Lindroos B, Suuronen R, Miettinen S. The Potential of Adipose Stem Cells in Regenerative
1163 Medicine. Stem Cell Rev. 2010;7:269–91.

1164 29. Kwon HM, Hur S-M, Park K-Y, Kim C-K, Kim Y-M, Kim H-S, et al. Multiple paracrine factors
1165 secreted by mesenchymal stem cells contribute to angiogenesis. Vascular Pharmacology.
1166 2014;63:19–28.

1167 30. Madrigal M, Rao KS, Riordan NH. A review of therapeutic effects of mesenchymal stem cell
1168 secretions and induction of secretory modification by different culture methods. J Transl Med.
1169 2014;12:71.

1170 31. Rennert RC, Januszyk M, Sorkin M, Rodrigues M, Maan ZN, Duscher D, et al. Microfluidic
1171 single-cell transcriptional analysis rationally identifies novel surface marker profiles to enhance
1172 cell-based therapies. Nat Commun. 2016;7:11945.

1173 32. Baer PC. Adipose-derived mesenchymal stromal/stem cells: An update on their phenotype in
1174 vivo and in vitro. World J Stem Cells. 2014;6:256.

1175 33. Mabuchi Y, Houlihan DD, Akazawa C, Okano H, Matsuzaki Y. Prospective Isolation of
1176 Murine and Human Bone Marrow Mesenchymal Stem Cells Based on Surface Markers. Stem
1177 Cells Int. 2013;2013:1–7.

1178 34. Dromard CC, Barreau C, Andr M, Berger-M ller S, Casteilla L, Planat-Benard V. Mouse
1179 adipose tissue stromal cells give rise to skeletal and cardiomyogenic cell sub-populations. Front
1180 Cell Dev Biol. 2014;2:697.

1181 35. Heneidi S, Simerman AA, Keller E, Singh P, Li X, Dumesic DA, et al. Awakened by Cellular
1182 Stress: Isolation and Characterization of a Novel Population of Pluripotent Stem Cells Derived
1183 from Human Adipose Tissue. Ljubimov AV, editor. PLoS ONE. 2013;8:e64752.

1184 36. Wachi H. Role of Elastic Fibers on Cardiovascular Disease. J. Health Sci. 2011;57:449–57.

1185 37. Hughes-Fulford M, Li C-F. The role of FGF-2 and BMP-2 in regulation of gene induction, cell
1186 proliferation and mineralization. J Orthop Surg Res. 2011;6:8.

1187 38. Kurimoto K. An improved single-cell cDNA amplification method for efficient high-density
1188 oligonucleotide microarray analysis. Nucleic Acids Res. 2006;34:e42–2.

1189 39. Yang L, Ma Z, Cao C, Zhang Y, Wu X, Lee R, et al. MR-Seq: measuring a single cell's
1190 transcriptome repeatedly by RNA-seq. Science Bulletin. 2017.

1191 40. Velten L, Haas SF, Raffel S, Blaszkiewicz S, Islam S, Hennig BP, et al. Human
1192 haematopoietic stem cell lineage commitment is a continuous process. Nat. Cell Biol.
1193 2017;Complex Sy:1695.

1194 41. Kowalczyk MS, Tirosh I, Heckl D, Rao TN, Dixit A, Haas BJ, et al. Single-cell RNA-seq
1195 reveals changes in cell cycle and differentiation programs upon aging of hematopoietic stem
1196 cells. Genome Res. 2015;25:1860–72.

1197 42. Wu AR, Neff NF, Kalisky T, Dalerba P, Treutlein B, Rothenberg ME, et al. Quantitative
1198 assessment of single-cell RNA-sequencing methods. Nat. Methods. 2013;11:41–6.

1199 43. Pauklin S, Vallier L. The Cell-Cycle State of Stem Cells Determines Cell Fate Propensity.
1200 Cell. 2013;155:135–47.

1201 44. Shimosato D, Shiki M, Niwa H. Extra-embryonic endoderm cells derived from ES cells
1202 induced by GATA Factors acquire the character of XEN cells. BMC Dev. Biol. 2007;7:80.

1203 45. Wagner F. GO-PCA: An Unsupervised Method to Explore Gene Expression Data Using Prior
1204 Knowledge. Li X, editor. PLoS ONE. 2015;10:e0143196.

1205 46. Yu G, He Q-Y. ReactomePA: an R/Bioconductor package for reactome pathway analysis
1206 and visualization. Mol. BioSyst. 2016;12:477–9.

1207 47. Tripathi S, Pohl MO, Zhou Y, Rodriguez-Frandsen A, Wang G, Stein DA, et al. Meta- and
1208 Orthogonal Integration of Influenza ?OMICs? Data Defines a Role for UBR4 in Virus Budding.
1209 Cell Host Microbe. 2015;18:723–35.

1210 48. Huang DW, Sherman BT, Lempicki RA. Systematic and integrative analysis of large gene
1211 lists using DAVID bioinformatics resources. Nat Protoc. 2008;4:44–57.

1212 49. Huang DW, Sherman BT, Lempicki RA. Bioinformatics enrichment tools: paths toward the
1213 comprehensive functional analysis of large gene lists. Nucleic Acids Res. 2008;37:1–13.

1214
1215
1216
1217
1218
1219
1220
1221
1222
1223
1224
1225
1226
1227

1228 **Figure titles and legends**

1229

1230 **Figure 1. Overview of Quartz-Seq2 experimental processes**

1231 Quartz-Seq2 consisted of five steps. (1) Each single cell in a droplet was sorted into lysis buffer
1232 in each well of a 384-well PCR plate using flow cytometry analysis data. (2) Poly-adenylated
1233 RNA in each well was reverse-transcribed into first-strand cDNA with reverse transcription
1234 primer, which had a unique cell barcode. We prepared 384 or 1,536 kinds of cell barcode (CB)
1235 with a unique sequence based on the Sequence–Levenshtein distance (SeqLv). The edit
1236 distance of SeqLv was 5. RT primer also had a UMI sequence for reduction of PCR bias (MB)
1237 and a poly-dT sequence for binding to poly-A RNA. (3) Cell barcode-labeled cDNAs from all 384
1238 wells were promptly collected by centrifugation using assembled collectors. (4) Collected
1239 first-strand cDNAs were purified and concentrated for subsequent whole-transcript amplification.
1240 In the poly-A tailing step, purified cDNA was extended with a poly-A tail by terminal
1241 deoxynucleotidyl transferase (TdT). Subsequently, second-strand cDNA was synthesized with a
1242 tagging primer, which had a poly-dT sequence. The resulting second-strand cDNA had a PCR
1243 primer sequence (M) at both ends of the cDNA. The cDNA was amplifiable at subsequent PCR
1244 amplification. (5) For conversion from amplified cDNA to sequence library DNA, we fragmented
1245 the amplified cDNA using the ultrasonicator Covaris. Such fragmented cDNA was ligated with a
1246 truncated Y-shaped sequence adaptor, which had an Illumina flow-cell binding sequence (P7)
1247 and a pool barcode sequence (PB). PB made it possible to mix different sets of
1248 cell-barcode-labeled cDNA. Ligated cDNA, which had CB and MB sequences, was enriched by
1249 PCR amplification. The resulting sequence library DNA contained P7 and P5 flow-cell binding
1250 sequences at respective ends of the DNA. We sequenced the cell-barcode site and the UMI site
1251 at Read1, the pool-barcode site at Index1, and the transcript sequence at Read2.

1252

1253 **Figure 2. Sequence performance of Quartz-Seq2 with molecular biological improvements**

1254 a) Improvement of poly-A tagging efficiency. Barplot represents the relative DNA yield in various
1255 poly-A tagging conditions using purified first-strand cDNA from 1 ng of total RNA. T55 buffer as
1256 the terminal deoxynucleotidyl transferase (TdT) buffer and the temperature condition “Increment”

1257 for the poly-A tagging step improved the cDNA yield of whole-transcript amplification. Buffer
1258 compositions were indicated in Additional file 4: Table S3. QuartzB represents use of a
1259 Quartz-Seq-like buffer as a positive control, in accordance with the approach described in the
1260 original Quartz-Seq paper. Finally, we quantified cDNA yield (300–9,000 bp) and byproduct DNA
1261 yield (50–300 bp) using Bioanalyzer (Agilent). (b) The improvement of cDNA yield with the
1262 combination of T55 buffer and "Increment" (T55+Inc) was confirmed by qPCR assay. We
1263 detected eight genes (*Eef1b2*, *Nanog*, *Pou5f1*, *Sox2*, *Utf1*, *Spp1*, *Ywhae*, *Tbp*) with amplified
1264 cDNA and nonamplified cDNA. We prepared nonamplified cDNA with 200 pg of total RNA and
1265 random hexamer. SCC stands for Spearman's rank correlation coefficient. c) Comparison
1266 between Quartz-Seq2 and Quartz-Seq-like conditions regarding sequence performance. We
1267 analyzed 384 wells with 10 pg of total RNA and used approximately 0.19 M fastq reads per well
1268 on average. We show the UMI count and gene count in barplots. We also show a diagrammatic
1269 depiction of the relationship between the cumulative number of detected genes and the gene
1270 expression level. d) Gene expression reproducibility between bulk poly-A-RNA-seq (1 μg of total
1271 RNA) and Quartz-Seq2 (10 pg of total RNA, averaged over 384 wells). e) The panels show a
1272 scatter plot between the mean of gene expression and the variability of gene expression with 10
1273 pg of total RNA in 384 wells. Red lines represent the theoretical variability of gene expression in
1274 the form of a Poisson distribution. The left and right panels represent the mean-CV plots before
1275 and after UMI filtering. The term "RT100" represents the condition of enzyme concentration in
1276 reverse transcription for Quartz-Seq2 (see Material and Methods).
1277
1278 **Figure 3. Cost reduction of Quartz-Seq2 upon improvement in quantitative performance**
1279 a) Reverse-transcription step has a highest share in single-cell experimental part of Quartz-Seq2.
1280 We present the different proportions of costs associated with each of the experimental steps.
1281 The reverse-transcription step accounts for approximately 65% of the total cost in the "RT100"
1282 condition. We thus established the "RT25" condition by reducing the enzyme concentration to
1283 25% in reverse transcription (for details, see Material and Methods). b) Barplots present the
1284 amount of amplified cDNA from three technical replicates of a 384-well plate with 10 pg of total
1285 RNA in all wells for the "RT100" and "RT25" conditions. The y-axis represents the yield of

1286 amplified cDNA. The cDNA yields from 10 pg of total RNA were 55.9 ± 5.5 ng for “RT100” and
1287 65.7 ± 2.5 ng for “RT25”. c) We analyzed amplified cDNA from 10 pg of total RNA by
1288 Quartz-Seq2 with various initial data sizes (approximately 0.27 M, 0.19 M, 0.171 M, 0.152 M,
1289 0.133 M, 0.114 M, 0.095 M, 0.076 M, 0.057 M, 0.038 M and 0.019 M fastq reads per 10 pg of
1290 total RNA on average) from NextSeq500. The Read2 length was 62 nt. In all panels, the x-axis
1291 represents the initial data size for one sample. We present the UMI count, gene count, and spike
1292 capture ratio in the upper panels. We also show the technical variability of the UMI count or gene
1293 count between wells in the lower panels. The y-axis presents the coefficient of variation of the
1294 UMI count or the gene count. d) Relationship between initial data size and the number of single
1295 cells for sequence analysis in NextSeq500 runs. Typically, one sequence run with NextSeq
1296 500/550 High Output v2 Kit reads out 400–450 M fastq reads. The x-axis represents the input
1297 cell number for one sequence run. The y-axis represents the initial data size (fastq reads) per
1298 cell on average. If we analyzed 4,000 single cells in one sequence run, approximately 0.1 M
1299 fastq reads on average would be assigned to one single cell. Red circle represents the typical
1300 range of shallow input read depth for a single cell. e) Capture ratio of ERCC spike mix I in the
1301 “RT25” condition. The capture ratio of ERCC spike-in mix I was 16.38±0.66% (n=3) at
1302 approximately 0.27 M fastq reads on average per well. The x-axis represents the copy number of
1303 input spike RNAs. The y-axis represents the averaged UMI count for ERCC spike RNAs.
1304
1305 **Figure 4. Quartz-Seq2 with high UMI conversion efficiency identified more marker genes**
1306 **and biological pathways**
1307 a) We defined the UMI counts divided by the raw fastq reads as the UMI conversion efficiency. b)
1308 UMI counts, gene counts, and UMI conversion efficiency for Quartz-Seq2 and Drop-seq2
1309 experiments. These values depended on the initial fastq reads. c) Venn diagram of genes that
1310 were differentially expressed between the ES cluster and the Dex-treated ES (PrE) cluster, as
1311 identified by Quartz-Seq2, Drop-seq, and bulk RNA-seq (left). The number of genes that differed
1312 in expression levels between ES and PrE cells by at least twofold was counted (FDR < 0.05). We
1313 also present a Venn diagram of the Reactome pathway (right). d) Venn diagram of GO terms for
1314 genes with highly variable expression, as identified by Quartz-Seq2 and Drop-seq.

1315

1316 **Figure 5. Quantitative comparison among Quartz-Seq2 and previously reported methods**
1317 **using embryonic stem cells**

1318 a) We determined the UMI and gene counts from 0.1 million fastq reads with Quartz-Seq2 in the
1319 "RT25" condition using a mixture of mouse ES cells and Dex-treated ES cells. In total, we
1320 analyzed one set of 384-well plates and three sets of 1,536-well plates using Quartz-Seq2. We
1321 also estimated the UMI conversion efficiency of other single-cell RNA-seq methods
1322 [CEL-seq2(C1), SCRB-seq, MARS-seq, and Drop-seq] from a previous study that used mouse
1323 ES cells [21]. In our comparison, the Read2 length for transcript mapping was 45 nt for all the
1324 methods, including Quartz-Seq2. To investigate the throughput capacity for establishing
1325 sequence library DNA, we estimated the number of processable single cells per $1,000 spent on
1326 each method: Quartz-Seq2 (384 indexes) yielded 1,818 cells, Quartz-Seq2 (1,536 indexes)
1327 yielded 2,500 cells, CEL-seq2(C1) yielded 111 cells, SCRB-seq yielded 500 cells, MARS-seq
1328 yielded 769 cells, and Drop-seq yielded 10,000 cells. The UMI conversion efficiency was 34.1%
1329 for Quartz-Seq2 (384 indexes), 34.4 ± 0.9% (n = 3) for Quartz-Seq2 (1,536 indexes), 22.4% for
1330 CEL-seq2(C1), 13.3% for SCRB-seq, 10.6% for MARS-seq, and 7.1% for Drop-seq. The
1331 average gene count was 6,673 for Quartz-Seq2 (384 indexes), 6,738 ± 57 (n = 3) for
1332 Quartz-Seq2 (1,536 indexes), 5,164 for CEL-seq2(C1), 4,044 for SCRB-seq, 3,252 for
1333 MARS-seq, and 2,738 for Drop-seq. b) We also estimated the average UMI and gene counts
1334 and the UMI conversion efficiency with various numbers of initial fastq reads for each method.
1335 The findings indicate that compared with the other methods, Quartz-Seq2 has a superior ability
1336 to detect UMI and gene counts from limited initial amounts of data (under 0.25 million fastq
1337 reads).

1338

1339 **Figure 6. Quartz-Seq2 analysis of 4,484 cells from mouse embryonic stem cells and**
1340 **differentiated cells**

1341 a) We successfully analyzed 97.3% of 4,608 wells. The procedures for cell suspension as used
1342 in this assay are shown. Cells cultured under ES-maintenance and Dex-treatment conditions
1343 were separately dissociated into single cells, stained with Hoechst 33342 and/or Calcein-AM,

1344 and mixed evenly. Calcein-AM-positive and -negative cells were sorted to 384-well plates in a
1345 checkered pattern. White scale bars represent 100 μm. b) Clustering of 4,484 single cells
1346 according to the transcriptome. Plotting of cells on t-SNE space with color labeling for each
1347 cluster. The percentage indicates the proportion of cells for each cluster relative to all cells
1348 analyzed. Numbers in parentheses indicate the numbers of cells making up the cluster. c)
1349 Marker genes for each cluster identified by Quart-Seq2. Cluster-specific or cluster-enriched
1350 genes were calculated for each cluster, and their expression is displayed as a color in a heatmap.
1351 No more than 50 cells are shown for simplicity. d) Reconstructed distribution of Calcein-AM
1352 intensity for each cluster. The x-axis represents the intensity of Calcein-AM dye staining. e)
1353 Reconstructed distribution of Hoechst 33342 intensity for each cluster. The y-axis represents the
1354 density of cells. The x-axis represents the intensity of Hoechst 33342 dye staining.
1355
1356 **Figure 7 Quartz-Seq2 analysis on two types of cell state: cell cycle-dependent and**
1357 **-independent cellular heterogeneity**
1358 a) Plotting cells on t-SNE space with the colors representing the intensity of Hoechst 33342
1359 staining. b) Dependency of expression of several genes on the intensity of Hoechst 33342
1360 staining [G2/M phase: *Ccnb1*; G1 phase: *Ccne1*; housekeeping gene: *Gnb2l1*; upper panels: ES
1361 main population (cluster 1); lower panels: PrE main population (cluster 4)]. c) Identification of cell
1362 cycle-associated genes. Average gene expression of cells in a bin is colored in the heatmap.
1363 Bins were arranged in order of Hoechst 33342 staining intensity. d) The number of cell
1364 cycle-associated genes identified for each z-threshold. e) Several examples for genes whose
1365 expression was variable, but not associated with the phase of the cell cycle. f) Single-cell qPCR
1366 detection of genes with variable expression.
1367
1368 **Figure 8 Quartz-Seq2 analysis of stromal vascular fraction (SVF) from mouse adipose**
1369 **tissue**
1370 a) Morphology of SVF cells. Adipose tissue from a cell suspension of SVF was prepared. Upper
1371 panels present a photograph of adipose tissues and dissociated SVF samples. Yellow scale bar
1372 represents 1 cm. White scale bar represents 10 μm. Lower panels represent the distribution of

1373 cell size information with different platforms (left: diameter of cell size using photography, right:
1374 flow cytometry information using a cell sorter). The diameter of cell size for SVF samples was
1375 6.43 ± 1.35 μm (n=200). b) Clustering of cells included in SVF. The transcriptome of
1376 approximately 1,000 cells was quantified by Quartz-Seq2 and clustering on t-SNE space was
1377 performed. In accordance with the genes and functional terms enriched in each cluster, the cell
1378 type was annotated. The percentage indicates the proportion of cells for each cluster relative to
1379 all cells analyzed. Numbers in parentheses indicate the numbers of cells constituting the cluster.
1380 c) Marker genes for each cluster were identified by Quart-Seq2. Cluster-specific or
1381 cluster-enriched genes were calculated for each cluster, with their expression being displayed as
1382 color in a heatmap. No more than 50 cells are shown for simplicity. d) The results of GO-PCA
1383 analysis. Functional terms enriched in the genes with high factor loadings of PCA were
1384 calculated and the enrichment is displayed as color in the heatmap. No more than 50 cells are
1385 shown for simplicity. e) Reactome pathway with genes differentially expressed between cluster 1
1386 and cluster 8.

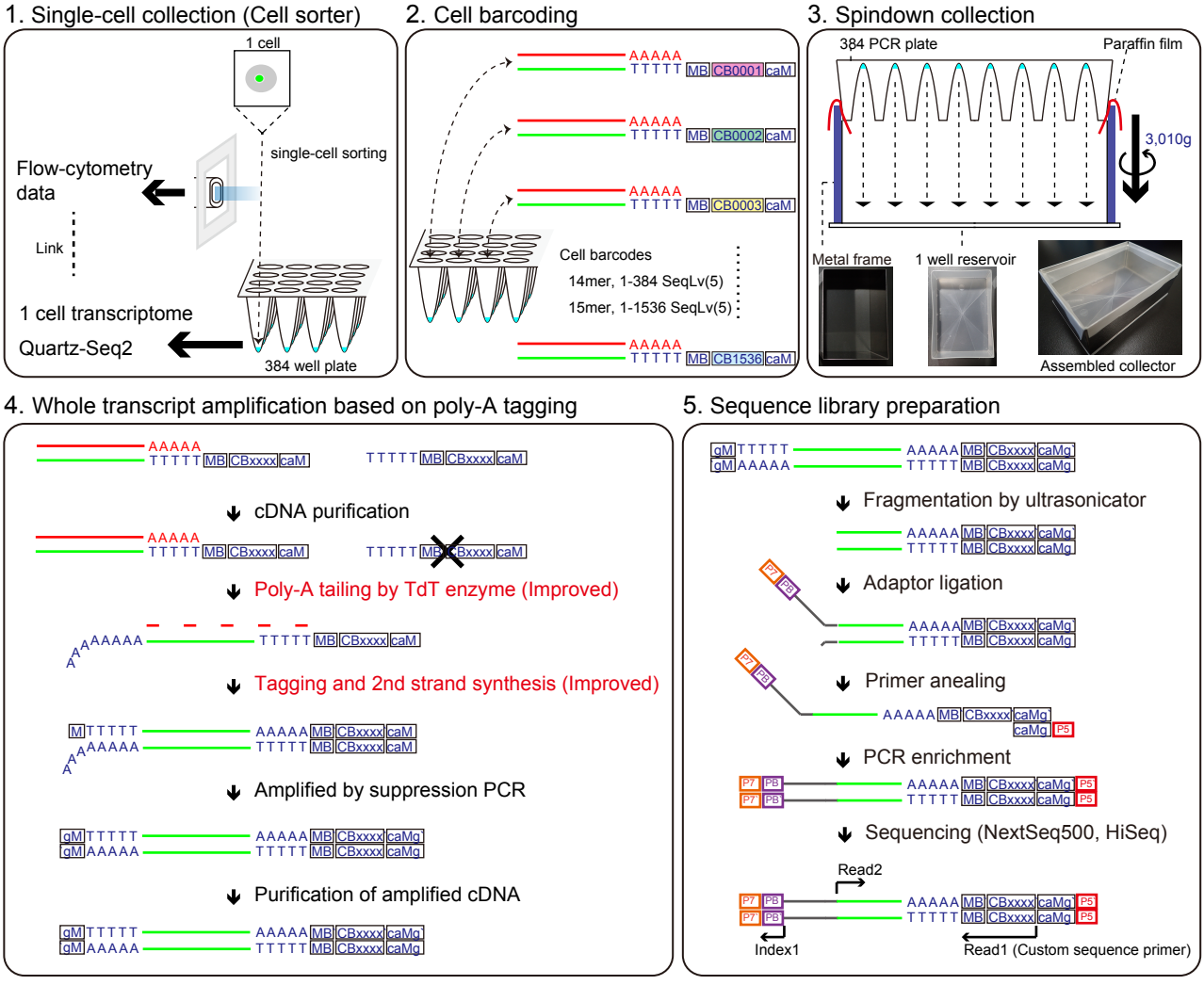
1. Single-cell collection (Cell sorter)
1 cell
single-cell sorting
Flow-cytometry data
Link
1 cell transcriptome
Quartz-Seq2
384 well plate
2. Cell barcoding
AAAAA
TTTTT MB CB0001 caM
TTTTT MB CB0002 caM
TTTTT MB CB0003 caM
TTTTT MB CB1536 caM
Cell barcodes
14mer, 1-384 SeqLv(5)
15mer, 1-1536 SeqLv(5)
3. Spindown collection
384 PCR plate
Paraffin film
3,010g
Metal frame
1 well reservoir
Assembled collector
4. Whole transcript amplification based on poly-A tagging
TTTTT MB CBxxxx caM
cDNA purification
Poly-A tailing by TdT enzyme (Improved)
Tagging and 2nd strand synthesis (Improved)
M TTTTT
Amplified by suppression PCR
gM TTTTT
gM AAAAA
Purification of amplified cDNA
5. Sequence library preparation
Fragmentation by ultrasonicator
Adaptor ligation
P7 PB
Primer anealing
PCR enrichment
P5
Sequencing (NextSeq500, HiSeq)
Read2
Index1
Read1 (Custom sequence primer)

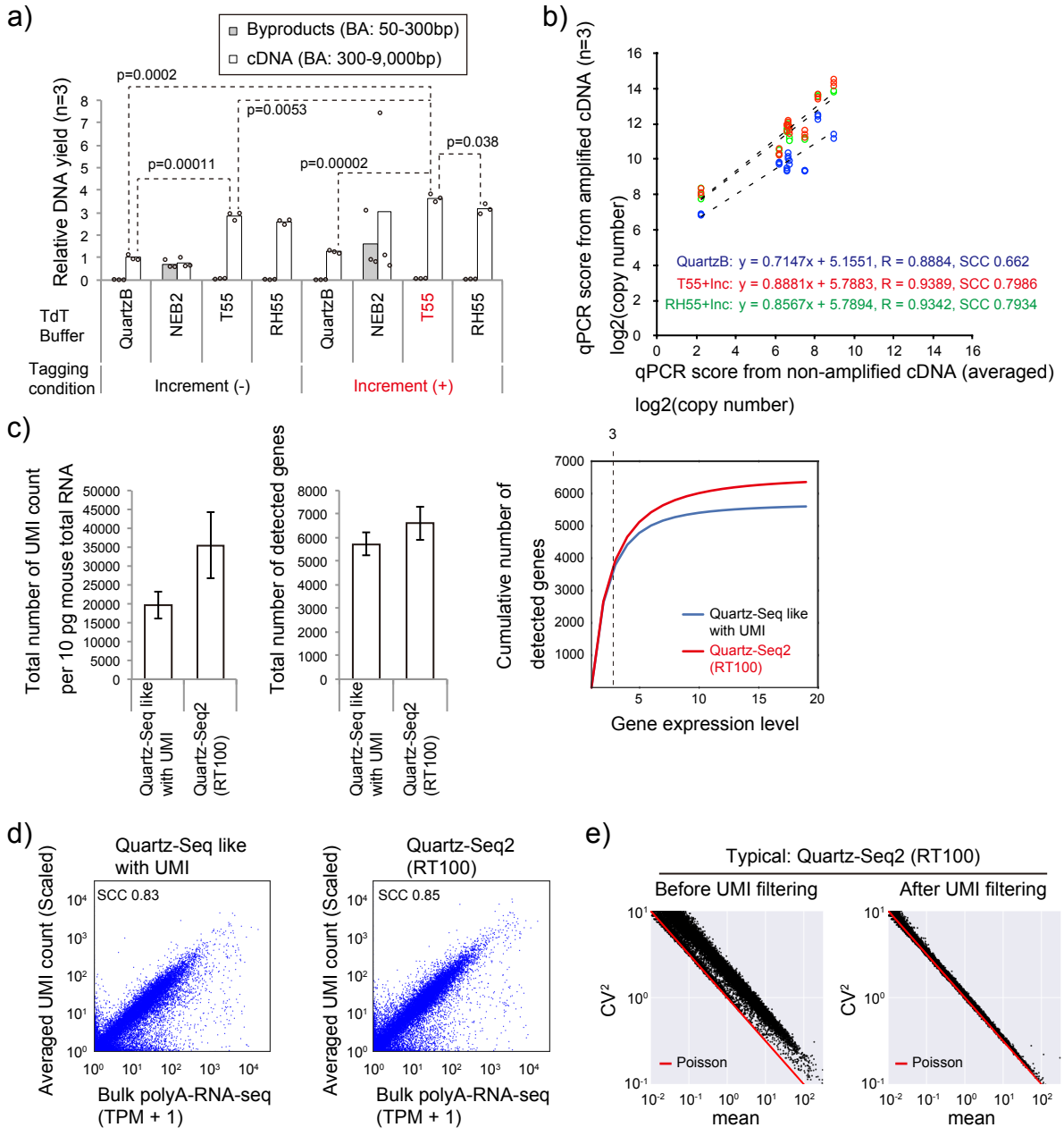
a)
Byproducts (BA: 50-300bp)
cDNA (BA: 300-9,000bp)
Relative DNA yield (n=3)
p=0.0002
p=0.0053
p=0.038
p=0.00011
p=0.00002
TdT Buffer
QuartzB
NEB2
T55
RH55
QuartzB
NEB2
T55
RH55
Tagging condition
Increment (-)
Increment (+)
b)
qPCR score from amplified cDNA (n=3)
log2(copy number)
QuartzB: y = 0.7147x + 5.1551, R = 0.8884, SCC 0.662
T55+Inc: y = 0.8881x + 5.7883, R = 0.9389, SCC 0.7986
RH55+Inc: y = 0.8567x + 5.7894, R = 0.9342, SCC 0.7934
qPCR score from non-amplified cDNA (averaged)
log2(copy number)
c)
Total number of UMI count per 10 pg mouse total RNA
Quartz-Seq like with UMI
Quartz-Seq2 (RT100)
Total number of detected genes
Quartz-Seq like with UMI
Quartz-Seq2 (RT100)
Cumulative number of detected genes
3
Quartz-Seq like with UMI
Quartz-Seq2 (RT100)
Gene expression level
d)
Quartz-Seq like with UMI
SCC 0.83
Averaged UMI count (Scaled)
Bulk polyA-RNA-seq (TPM + 1)
Quartz-Seq2 (RT100)
SCC 0.85
Averaged UMI count (Scaled)
Bulk polyA-RNA-seq (TPM + 1)
e)
Typical: Quartz-Seq2 (RT100)
Before UMI filtering
After UMI filtering
CV²
Poisson
mean
CV²
Poisson
mean

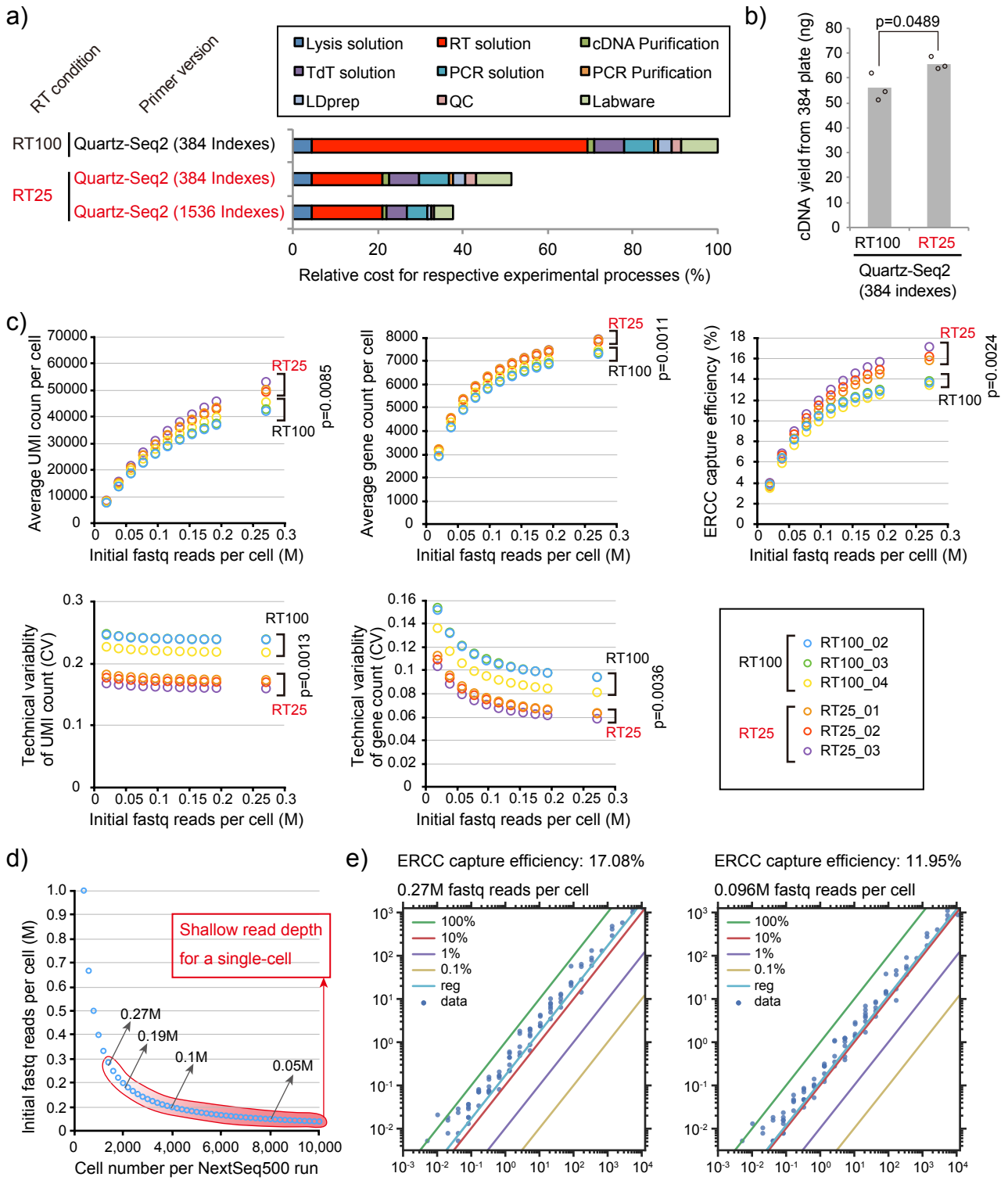
a)
RT condition
Primer version
Lysis solution
RT solution
cDNA Purification
TdT solution
PCR solution
PCR Purification
LDprep
QC
Labware
RT100
Quartz-Seq2 (384 Indexes)
RT25
Quartz-Seq2 (384 Indexes)
Quartz-Seq2 (1536 Indexes)
Relative cost for respective experimental processes (%)
b)
p=0.0489
cDNA yield from 384 plate (ng)
RT100
RT25
Quartz-Seq2 (384 indexes)
c)
Average UMI coun per cell
Initial fastq reads per cell (M)
p=0.0085
Average gene count per cell
p=0.0011
ERCC capture efficiency (%)
Initial fastq reads per celll (M)
p=0.0024
Technical variablity of UMI count (CV)
p=0.0013
Technical variablity of gene count (CV)
p=0.0036
RT100_02
RT100_03
RT100_04
RT25_01
RT25_02
RT25_03
d)
Initial fastq reads per cell (M)
Shallow read depth for a single-cell
0.27M
0.19M
0.1M
0.05M
Cell number per NextSeq500 run
e)
ERCC capture efficiency: 17.08%
0.27M fastq reads per cell
ERCC capture efficiency: 11.95%
0.096M fastq reads per cell
100%
10%
1%
0.1%
reg
data

a)

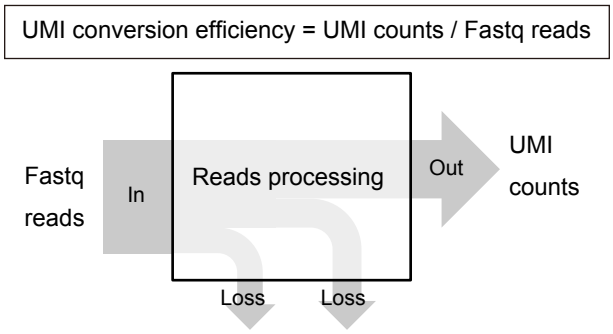
UMI conversion efficiency = UMI counts / Fastq reads
Fastq reads
In
Reads processing
Out
UMI counts
Loss
Loss

b)

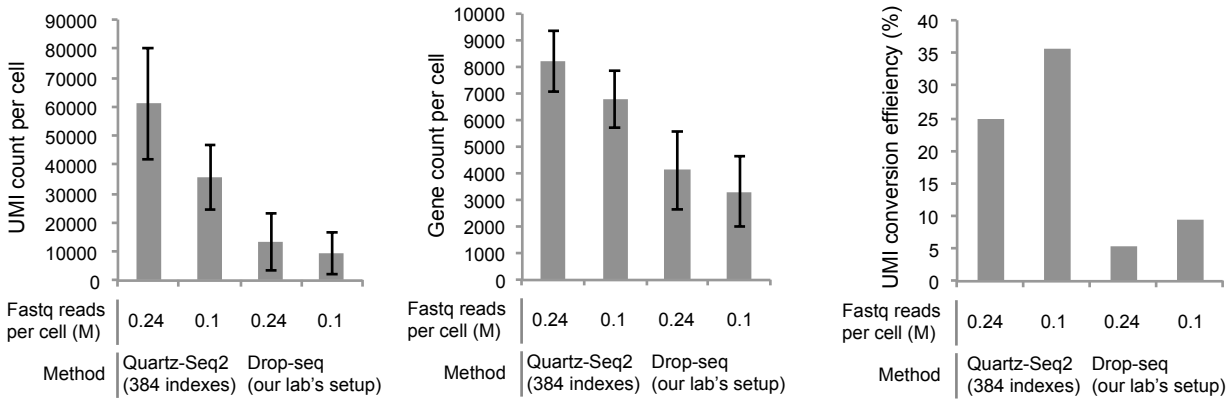
UMI count per cell
90000
80000
70000
60000
50000
40000
30000
20000
10000
0
Gene count per cell
10000
9000
8000
7000
6000
5000
4000
3000
2000
1000
0
UMI conversion effieiency (%)
40
35
30
25
20
15
10
5
0
Fastq reads per cell (M)
0.24
0.1
0.24
0.1
Method
Quartz-Seq2 (384 indexes)
Drop-seq (our lab's setup)

c)

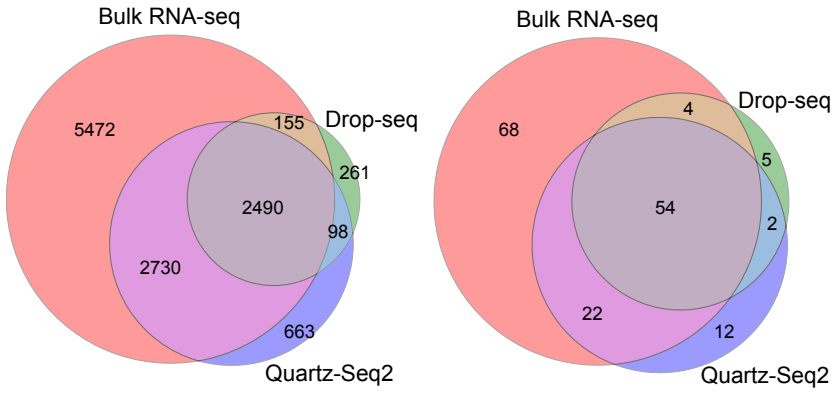
Differentially expressed genes
Bulk RNA-seq
Drop-seq
Quartz-Seq2
5472
155
261
2490
98
2730
663
Reactome pathway
Bulk RNA-seq
Drop-seq
Quartz-Seq2
68
4
5
54
2
22
12

d)

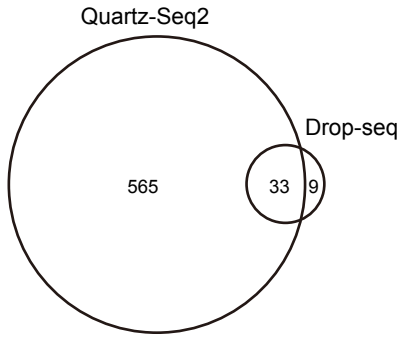
GO terms
on highly variable genes
Quartz-Seq2
Drop-seq
565
33
9

a)

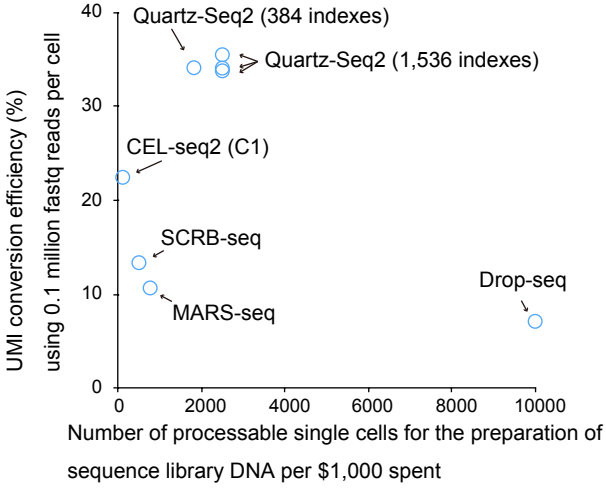
Quartz-Seq2 (384 indexes)
Quartz-Seq2 (1,536 indexes)
CEL-seq2 (C1)
SCRB-seq
MARS-seq
Drop-seq
UMI conversion efficiency (%)
using 0.1 million fastq reads per cell
Number of processable single cells for the preparation of
sequence library DNA per $1,000 spent

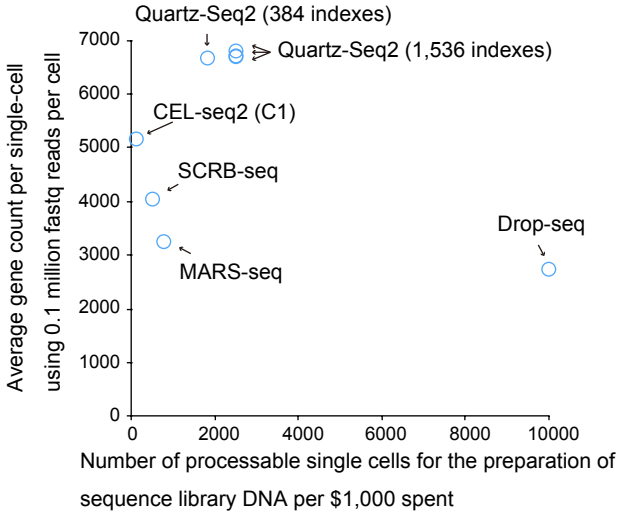
Quartz-Seq2 (384 indexes)
Quartz-Seq2 (1,536 indexes)
CEL-seq2 (C1)
SCRB-seq
MARS-seq
Drop-seq
Average gene count per single-cell
using 0.1 million fastq reads per cell
Number of processable single cells for the preparation of
sequence library DNA per $1,000 spent

b)

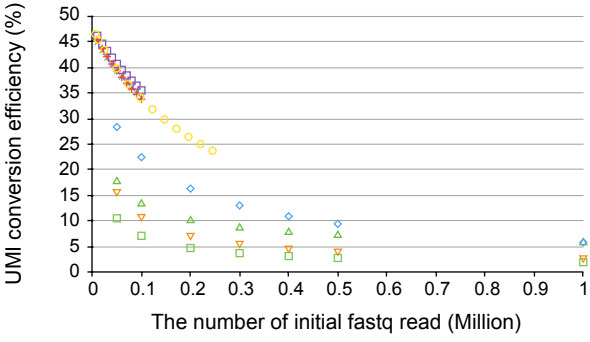
UMI conversion efficiency (%)
The number of initial fastq read (Million)

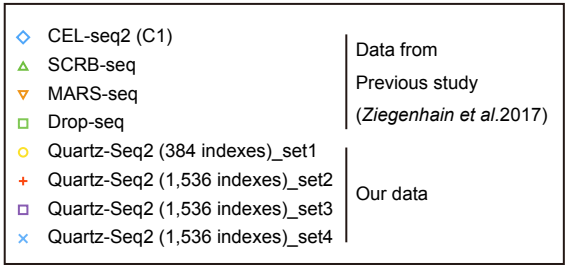
CEL-seq2 (C1)
SCRB-seq
MARS-seq
Drop-seq
Quartz-Seq2 (384 indexes)_set1
Quartz-Seq2 (1,536 indexes)_set2
Quartz-Seq2 (1,536 indexes)_set3
Quartz-Seq2 (1,536 indexes)_set4
Data from
Previous study
(Ziegenhain et al.2017)
Our data

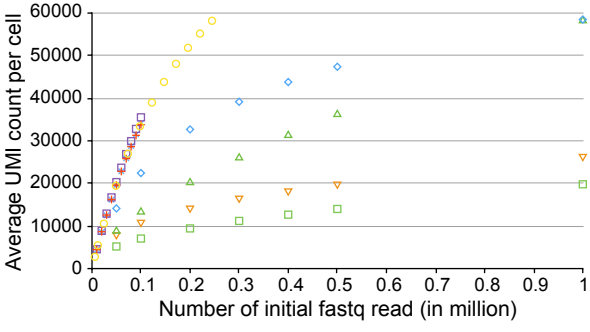
Average UMI count per cell
Number of initial fastq read (in million)

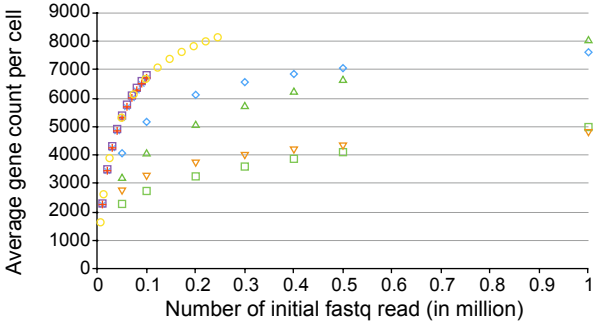
Average gene count per cell
Number of initial fastq read (in million)

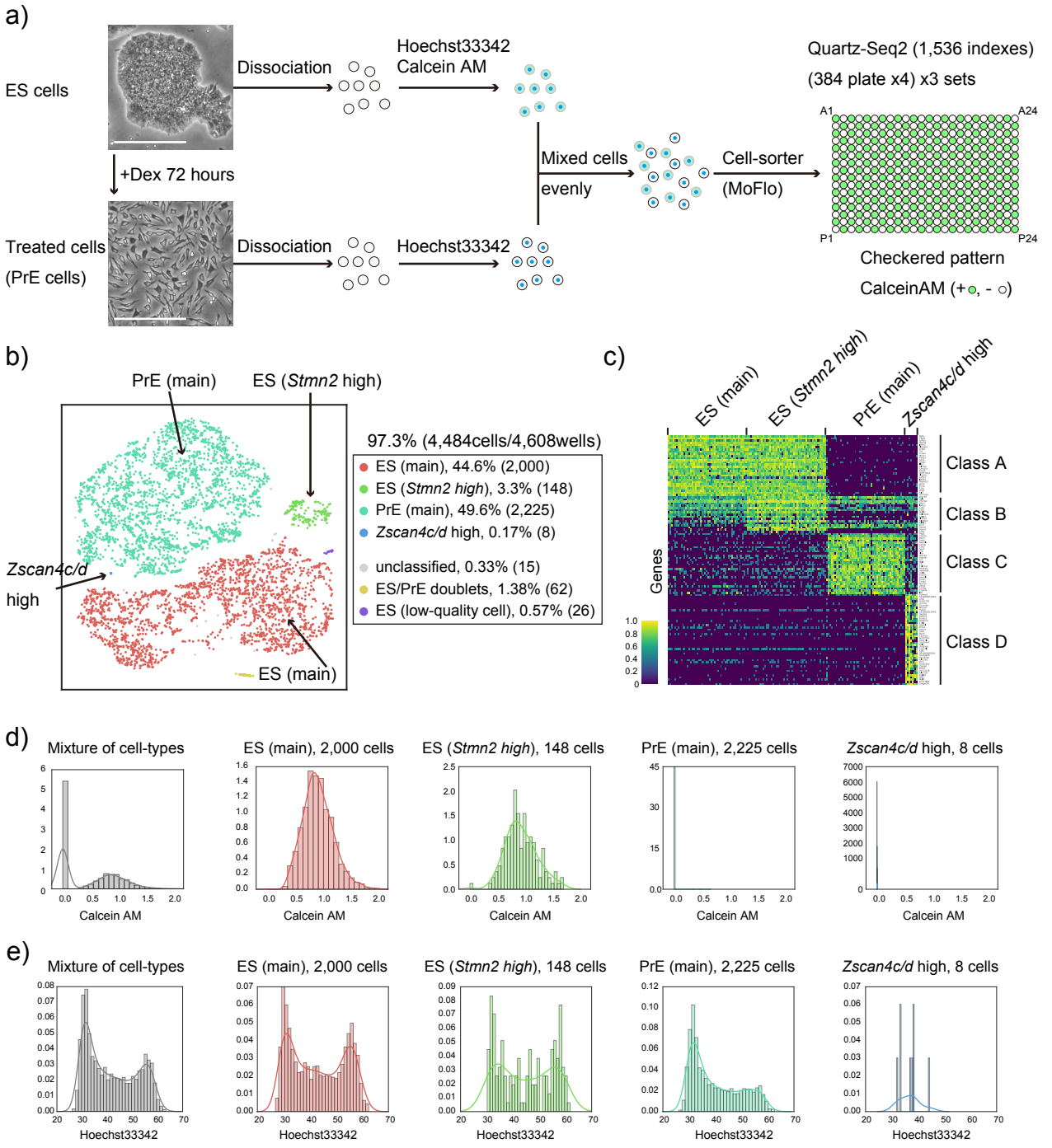
a)
ES cells
Dissociation
Hoechst33342
Calcein AM
+Dex 72 hours
Treated cells
(PrE cells)
Dissociation
Hoechst33342
Mixed cells
evenly
Cell-sorter
(MoFlo)
Quartz-Seq2 (1,536 indexes)
(384 plate x4) x3 sets
A1
A24
P1
P24
Checkered pattern
CalceinAM (+, - )
b)
PrE (main)
ES (Stmn2 high)
Zscan4c/d
high
ES (main)
97.3% (4,484cells/4,608wells)
ES (main), 44.6% (2,000)
ES (Stmn2 high), 3.3% (148)
PrE (main), 49.6% (2,225)
Zscan4c/d high, 0.17% (8)
unclassified, 0.33% (15)
ES/PrE doublets, 1.38% (62)
ES (low-quality cell), 0.57% (26)
c)
ES (main)
ES (Stmn2 high)
PrE (main)
Zscan4c/d high
Genes
Class A
Class B
Class C
Class D
d)
Mixture of cell-types
ES (main), 2,000 cells
ES (Stmn2 high), 148 cells
PrE (main), 2,225 cells
Zscan4c/d high, 8 cells
Calcein AM
e)
Mixture of cell-types
ES (main), 2,000 cells
ES (Stmn2 high), 148 cells
PrE (main), 2,225 cells
Zscan4c/d high, 8 cells
Hoechst33342

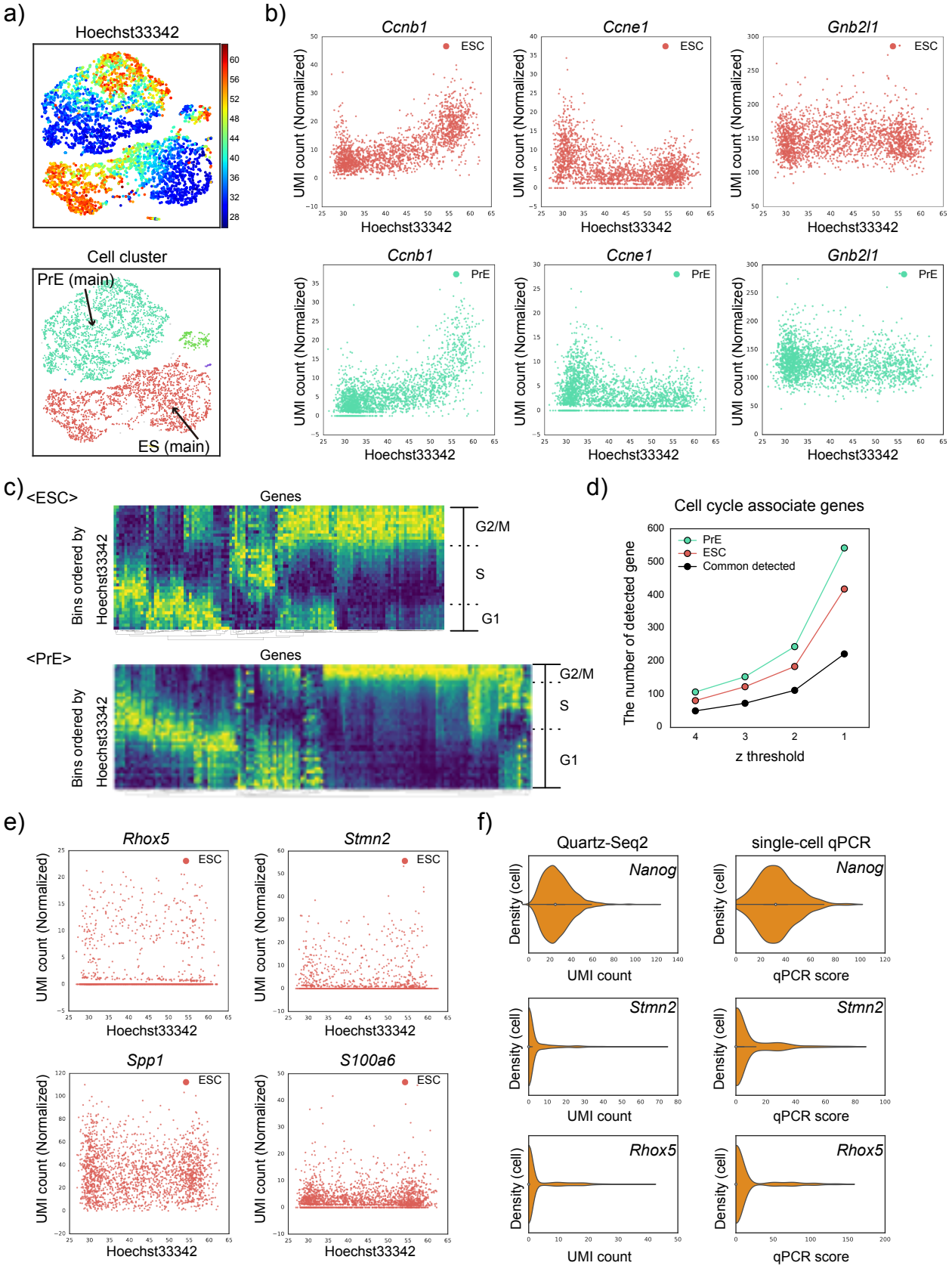
a)
Hoechst33342
Cell cluster
PrE (main)
ES (main)
b)
Ccnb1
Ccne1
Gnb2l1
ESC
PrE
UMI count (Normalized)
Hoechst33342
c)
<ESC>
<PrE>
Genes
Bins ordered by Hoechst33342
G2/M
S
G1
d)
Cell cycle associate genes
PrE
ESC
Common detected
The number of detected gene
z threshold
e)
Rhox5
Stmn2
Spp1
S100a6
ESC
UMI count (Normalized)
Hoechst33342
f)
Quartz-Seq2
single-cell qPCR
Nanog
Stmn2
Rhox5
Density (cell)
UMI count
qPCR score

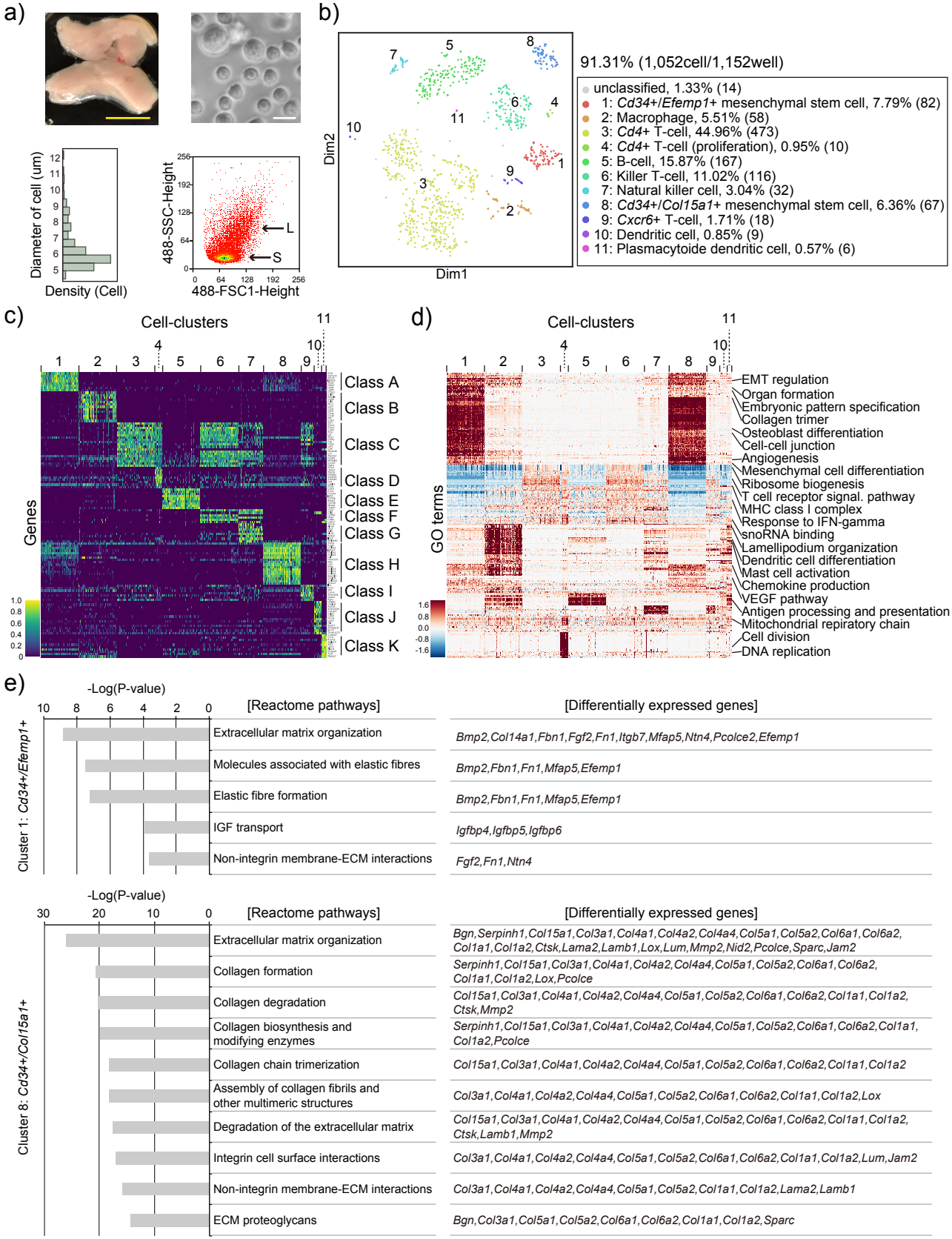
a)
Diameter of cell (um)
Density (Cell)
488-SSC-Height
488-FSC1-Height
L
S
b)
Dim1
Dim2
91.31% (1,052cell/1,152well)
unclassified, 1.33% (14)
1: Cd34+/Efemp1+ mesenchymal stem cell, 7.79% (82)
2: Macrophage, 5.51% (58)
3: Cd4+ T-cell, 44.96% (473)
4: Cd4+ T-cell (proliferation), 0.95% (10)
5: B-cell, 15.87% (167)
6: Killer T-cell, 11.02% (116)
7: Natural killer cell, 3.04% (32)
8: Cd34+/Col15a1+ mesenchymal stem cell, 6.36% (67)
9: Cxcr6+ T-cell, 1.71% (18)
10: Dendritic cell, 0.85% (9)
11: Plasmacytoide dendritic cell, 0.57% (6)
c)
Cell-clusters
Genes
Class A
Class B
Class C
Class D
Class E
Class F
Class G
Class H
Class I
Class J
Class K
d)
Cell-clusters
GO terms
EMT regulation
Organ formation
Embryonic pattern specification
Collagen trimer
Osteoblast differentiation
Cell-cell junction
Angiogenesis
Mesenchymal cell differentiation
Ribosome biogenesis
T cell receptor signal. pathway
MHC class I complex
Response to IFN-gamma
snoRNA binding
Lamellipodium organization
Dendritic cell differentiation
Mast cell activation
Chemokine production
VEGF pathway
Antigen processing and presentation
Mitochondrial repiratory chain
Cell division
DNA replication
e)
-Log(P-value)
[Reactome pathways]
[Differentially expressed genes]
Cluster 1: Cd34+/Efemp1+
Extracellular matrix organization
Bmp2,Col14a1,Fbn1,Fgf2,Fn1,Itgb7,Mfap5,Ntn4,Pcolce2,Efemp1
Molecules associated with elastic fibres
Bmp2,Fbn1,Fn1,Mfap5,Efemp1
Elastic fibre formation
Bmp2,Fbn1,Fn1,Mfap5,Efemp1
IGF transport
Igfbp4,Igfbp5,Igfbp6
Non-integrin membrane-ECM interactions
Fgf2,Fn1,Ntn4
Cluster 8: Cd34+/Col15a1+
Extracellular matrix organization
Bgn,Serpinh1,Col15a1,Col3a1,Col4a1,Col4a2,Col4a4,Col5a1,Col5a2,Col6a1,Col6a2,Col1a1,Col1a2,Ctsk,Lama2,Lamb1,Lox,Lum,Mmp2,Nid2,Pcolce,Sparc,Jam2
Collagen formation
Serpinh1,Col15a1,Col3a1,Col4a1,Col4a2,Col4a4,Col5a1,Col5a2,Col6a1,Col6a2,Col1a1,Col1a2,Lox,Pcolce
Collagen degradation
Col15a1,Col3a1,Col4a1,Col4a2,Col4a4,Col5a1,Col5a2,Col6a1,Col6a2,Col1a1,Col1a2,Ctsk,Mmp2
Collagen biosynthesis and modifying enzymes
Serpinh1,Col15a1,Col3a1,Col4a1,Col4a2,Col4a4,Col5a1,Col5a2,Col6a1,Col6a2,Col1a1,Col1a2,Pcolce
Collagen chain trimerization
Col15a1,Col3a1,Col4a1,Col4a2,Col4a4,Col5a1,Col5a2,Col6a1,Col6a2,Col1a1,Col1a2
Assembly of collagen fibrils and other multimeric structures
Col3a1,Col4a1,Col4a2,Col4a4,Col5a1,Col5a2,Col6a1,Col6a2,Col1a1,Col1a2,Lox
Degradation of the extracellular matrix
Col15a1,Col3a1,Col4a1,Col4a2,Col4a4,Col5a1,Col5a2,Col6a1,Col6a2,Col1a1,Col1a2,Ctsk,Lamb1,Mmp2
Integrin cell surface interactions
Col3a1,Col4a1,Col4a2,Col4a4,Col5a1,Col5a2,Col6a1,Col6a2,Col1a1,Col1a2,Lum,Jam2
Non-integrin membrane-ECM interactions
Col3a1,Col4a1,Col4a2,Col4a4,Col5a1,Col5a2,Col1a1,Col1a2,Lama2,Lamb1
ECM proteoglycans
Bgn,Col3a1,Col5a1,Col5a2,Col6a1,Col6a2,Col1a1,Col1a2,Sparc